A *GLB1* transgene with enhanced therapeutic potential for the preclinical development of *ex-vivo* gene therapy to treat mucopolysaccharidosis type IVB

Stefania Crippa,[1] Gaia Alberti,[1] Laura Passerini,[1] Evelyn Oliva Savoia,[1] Marilena Mancino,[1] Giada De Ponti,[1] Ludovica Santi,[1] Margherita Berti,[1] Marialuisa Testa,[2] Raisa Jofra Hernandez,[1] Pamela Quaranta,[1] Selene Ceriotti,[1] Ilaria Visigalli,[3] Amelia Morrone,[4,5] Antonella Paoli,[4] Claudia Forni,[6] Serena Scala,[1] Massimo Degano,[7,8] Leopoldo Staiano,[2,9] Silvia Gregori,[1] Alessandro Aiuti,[1,8,10] and Maria Ester Bernardo[1,8,10]

[1]San Raffaele Telethon Institute for Gene Therapy (SR-TIGET), IRCCS San Raffaele Scientific Institute, 20132 Milan, Italy; [2]Telethon Institute of Genetics and Medicine (TIGEM), 80078 Naples, Italy; [3]GLP - San Raffaele Telethon Institute for Gene Therapy (SR-TIGET), IRCCS San Raffaele Scientific Institute, 20132 Milan, Italy; [4]Laboratory of Molecular Biology of Neurometabolic Diseases, Neuroscience Department, Meyer Children's Hospital IRCCS, 50139 Florence, Italy; [5]Department of Neurosciences, Psychology, Drug Research and Child Health (NEUROFARBA), University of Florence, 50139 Florence, Italy; [6]Telethon Foundation, 00185 Rome, Italy; [7]Biocrystallography Unit, IRCCS San Raffaele Scientific Institute, 20132 Milan, Italy; [8]Università Vita-Salute San Raffaele, 20132 Milan, Italy; [9]Institute for Genetic and Biomedical Research, National Research Council (CNR), 20138 Milan, Italy; [10]Pediatric Immunohematology and Bone Marrow Transplantation Unit, IRCCS San Raffaele Scientific Institute, 20132 Milan, Italy

Mucopolysaccharidosis type IVB (MPSIVB) is a lysosomal storage disorder caused by β-galactosidase (β-GAL) deficiency characterized by severe skeletal and neurological alterations without approved treatments. To develop hematopoietic stem progenitor cell (HSPC) gene therapy (GT) for MPSIVB, we designed lentiviral vectors (LVs) encoding human β-GAL to achieve supraphysiological release of the therapeutic enzyme in human HSPCs and metabolic correction of diseased cells. Transduced HSPCs displayed proper colony formation, proliferation, and differentiation capacity, but their progeny failed to release the enzyme at supraphysiological levels. Therefore, we tested alternative LVs to overexpress an enhanced β-GAL deriving from murine (LV-enhGLB1) and human selectively mutated GLB1 sequences (LV-mutGLB1). Only human HSPCs transduced with LV-enhGLB1 overexpressed β-GAL *in vitro* and *in vivo* without evidence of overexpression-related toxicity. Their hematopoietic progeny efficiently released β-GAL, allowing the cross-correction of defective cells, including skeletal cells. We found that the low levels of human GLB1 mRNA in human hematopoietic cells and the improved stability of the enhanced β-GAL contribute to the increased efficacy of LV-enhGLB1. Importantly, the enhanced β-GAL enzyme showed physiological lysosomal trafficking in human cells and was not associated with increased immunogenicity *in vitro*. These results support the use of LV-enhGLB1 for further HSPC-GT development and future clinical translation to treat MPSIVB multisystem disease.

INTRODUCTION

Mucopolysaccharidosis type IVB (MPSIVB) is a rare inherited lysosomal storage disorder (LSD) caused by β-galactosidase (β-GAL) deficiency. The human *GLB1* gene (3p21.33) encodes for the lysosomal enzyme β-GAL, a hydrolase involved in the degradation of keratan sulfate (KS), and for a membrane receptor named elastin binding protein (EBP) by alternative splicing.[1,2] KS is mainly present in the cartilage, bone, and cornea and is synthesized in the central nervous system during development and glial scar formation upon injury.[3–5] The β-GAL deficiency causes the accumulation of undigested KS in the lysosomes, leading to severe skeletal and ligament alterations. The principal skeletal alterations in MPSIVB patients are short stature with a disproportionally short trunk with variable degrees of kyphoscoliosis, pectus carinatum, large appearing head with midface hypoplasia and mandibular protrusion, hyperextensible joints, coxa and genua valga, and flat feet. Corneal clouding and cardiac valve disease are additional findings.[2,6,7] Three common pathogenic variants have been associated with pure skeletal disease (MPSIVB or Morquio syndrome B): p.Tyr83His, p.Thr500Ala, and p.Trp273Leu.[8,9] In contrast, most of the GLB1 gene-related pathogenic variants are associated with the additional manifestation of a range of rapidly progressive to attenuated courses of neurodegeneration with the clinical characteristics of GM1 gangliosidosis. MPSIVB has a prevalence of 1 in 250,000 and a carrier frequency of 1 in 250, while the worldwide incidence of GM1-gangliosidosis is 1 in 100,000, with a carrier frequency of 1 in 160.[10–12] There are currently no approved therapies for MPSIVB and GM1 gangliosidosis patients, and current approaches involve

Correspondence: Alessandro Aiuti, San Raffaele Telethon Institute for Gene Therapy (SR-TIGET), IRCCS San Raffaele Scientific Institute, 20132 Milan, Italy.
E-mail: aiuti.alessandro@hsr.it

interdisciplinary collaboration to provide supportive therapies and targeted management for specific symptoms. Previous works showed a low stability of the human β-GAL in the extracellular environment,[13–15] therefore challenging the establishment of LSD conventional therapies based on the enzyme uptake by diseased cells from external sources, such as enzyme replacement therapy (ERT) and allogeneic hematopoietic stem and progenitor cell transplantation (HSCT). In addition, the ERT developed for other LSDs shows several disadvantages, including the short half-life of the recombinant enzyme, the patient's immune reaction, and the limited accessibility to poorly vascularized or barrier-protected tissues, limiting its therapeutic efficacy on the skeletal and neurological manifestations.[16–18] Despite HSCT being considered the standard of care for some LSDs, the skeleton, heart valves, and central nervous system remain refractory to metabolic correction post-HSCT. In addition, the functional outcome of HSCT depends on the patient's age and the state of the disease at the time of the intervention; moreover, HSCT remains associated with short- and long-term risks, including rejection and graft-versus-host disease, and is limited by donor availability.[19–21] Several studies have demonstrated that hematopoietic stem progenitor cell (HSPC) gene therapy (GT) approaches can overcome some of these limitations, showing safety and efficacy in inducing metabolic correction of non-hematopoietic tissues in preclinical models of LSDs and clinical trials.[22–27] Clinical data of HSPC-GT in metachromatic leukodystrophy (MLD) patients (NCT01560182) demonstrated the treatment efficacy on neurological symptoms, including preservation of cognitive and motor functions.[28] More recently, results of the phase I/II clinical trial of autologous lentiviral vector (LV)-based HSPC-GT for mucopolysaccharidosis type I Hurler (MPSI-H) patients (NCT03488394) demonstrated supraphysiologic levels of therapeutic enzyme in patients' blood associated with a rapid normalization of urinary glycosaminoglycan excretion and rapid clearance of anti-enzyme immunoglobulin G. The early clinical outcome indicates growth tracking in line with peers, resolution of joint stiffness and stability of spinal and hip abnormalities, and attenuation of neurological symptoms.[25,29] Altogether, these data suggest that gene-corrected HSPCs generate circulating and tissue-resident cells, which release supraphysiological levels of the therapeutic enzyme capable of cross-correcting tissues of non-hematopoietic origin, including brain and skeletal cells that are not targeted by the conventional approved therapies. Based on common clinical and pathogenetic features of LSDs, we reasoned that the HSPC-GT-mediated correction mechanism could also be applied to MPSIVB and GM1 gangliosidosis, characterized by severe skeletal and neurological involvement, respectively. Thus, we generated different third-generation LVs encoding for human and murine-derived β-GAL and evaluated their toxicity in human HSPCs *in vitro* and in an *in vivo* biodistribution model. We further proved the cross-correction principle in different 2D *in vitro* models. Our data indicate that only HSPCs engineered to overexpress the murine-derived enzyme with enhanced stability are capable of cross-correcting patients' cells at a therapeutic level in the absence of toxicity, supporting the further development of HSPC-GT and future clinical approaches for treating MPSIVB and GM1 -gangliosidosis using the murine-derived *GLB1* gene.

RESULTS

A LV encoding for the human β-GAL fails to induce supraphysiological release of the therapeutic enzyme from transduced human HSPCs

Based on previous preclinical and clinical data in other LSDs,[23–25,28] we generated at a preclinical level third-generation LVs to overexpress the human β-GAL in CD34^{+} HSPCs collected upon mobilization with granulocyte colony-stimulating factor (G-CSF) from the peripheral blood (mPB) of healthy donors with the ultimate goal to establish an HSPC-GT approach for GM1-related disorders. We cloned the human *GLB1* gene (NM_000404.4) into the LV construct successfully employed in the MPSI-H-GT clinical trial conducted at our Institute (NCT03488394)[25] in which the transgene is under the control of the human PGK promoter, a moderately active cellular promoter with excellent safety records (LV-hGLB1 WT).[30,31] We also cloned a codon-optimized version of the human *GLB1* transgene (LV-hGLB1 OPT) that may improve the enzyme expression (Table S1). Human mPB CD34^{+} cells from healthy donors were transduced with these LVs at different multiplicity of infection (MOI) (100, 30, 10) using a single hit transduction protocol in the presence of cyclosporin H (CsH) as transduction enhancer.[32] We analyzed the efficiency of transduction and the related toxicity compared with untransduced (UT) cells (Figure S1A). We did not observe alterations in the colony number and composition of transduced HSPCs and there was no impact on cell proliferation when transduced HSPCs were cultured in myeloid-skewing conditions (liquid culture) (Figures 1A and 1B). The percentage of transduction in progenitor cells was slightly higher when using the LV-hGLB1 OPT compared with the LV-hGLB1 WT (Figure 1C), while the mean vector copy number (VCN) measured on single colonies (Figure S1B) and on the myeloid liquid culture (Figure 1D) were similar.

Next, we evaluated the level of β-GAL expression in transduced cells compared with UT controls by western blot (WB) analysis and we measured β-GAL activity in the cell pellet and extracellular medium of HSPC-derived myeloid cells. The lysosomal form of the β-GAL (64 kDa) was overexpressed in the transduced cells (Figure 1E), leading to an increased intracellular enzymatic activity compared with UT controls (Figure 1F). On the contrary, we did not detect β-GAL in the extracellular medium (Figure 1E) and we measured only an average of 2-fold increase of β-GAL activity in cell supernatants (conditioned medium [CM]) from transduced cells at MOI of 30 and 100, with no difference between LV-hGLB1 WT and OPT (Figure 1G). We further tested the LV-hGLB1 (WT and OPT) efficacy in a 2D *in vitro* system. MPSIVB patient fibroblasts were used as target cells and exposed for 12 h to the CM from UT or LV-hGLB1 transduced myeloid cells (Figure 2A). As shown in Figure 2B, the level of β-GAL activity measured in patients' fibroblasts treated with the CM from LV-hGLB1 WT and OPT transduced cells was not significantly higher compared with treatment with the CM from UT HSPCs. We concluded that both LV constructs are unsuitable to induce the release of the therapeutic enzyme from gene-corrected human HSPCs at supraphysiological levels required for metabolic correction of β-GAL-deficient cells.
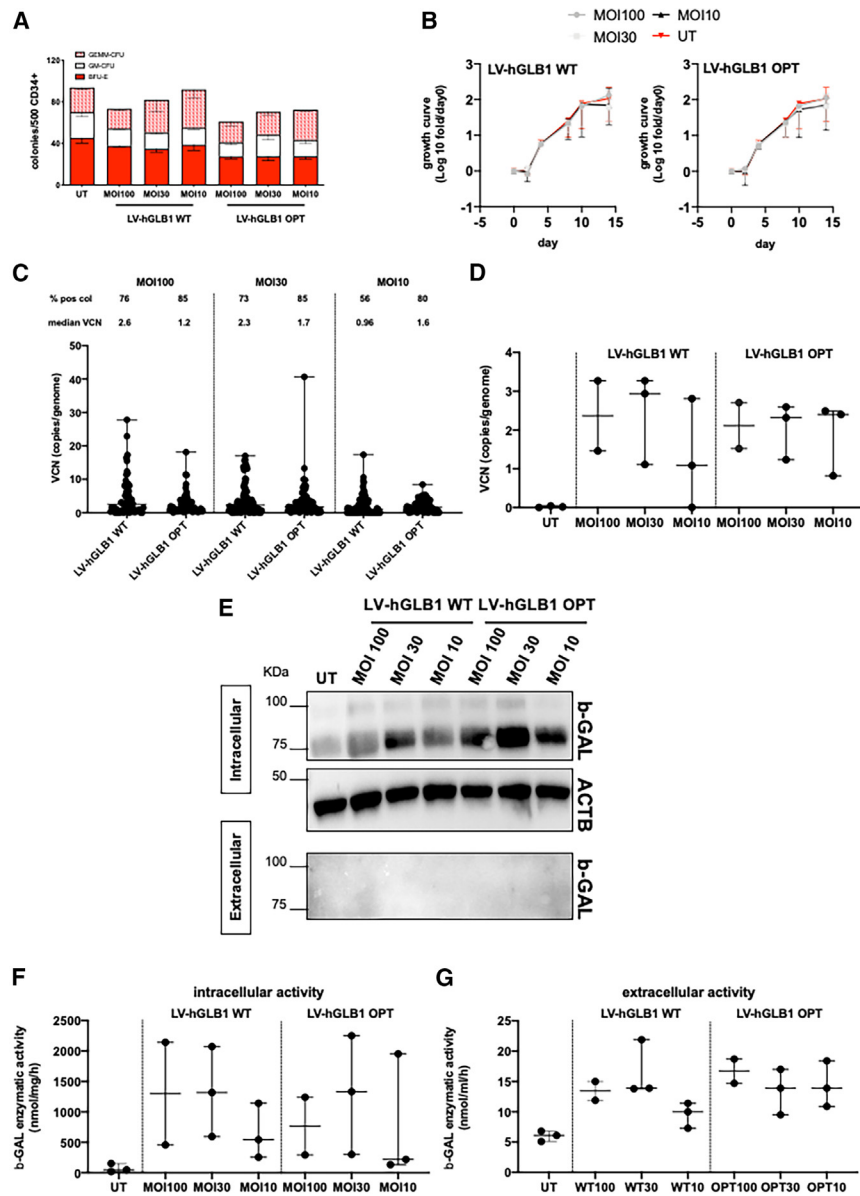
Figure 1. *In vitro* testing of lentiviral vectors encoding for human β-GAL

Data were collected for $n = 3$ HSPC samples transduced at an MOI of 30 and 10, and for $n = 2$ HSPC sample transduced at an MOI of 100. Statistical analyses were performed on samples transduced at an MOI of 30 and 10 compared with untransduced (UT) cells. (A) Colony formation assay of mobilized peripheral blood CD34+ cells transduced at different MOI (100, 30, 10) with the lentiviral vector bearing the wild-type (LV-hGLB1 WT) and codon-optimized (LV-hGLB1 OPT) cDNA sequence encoding for the human β-galactosidase. UT cells were used as controls to determine the potential toxic effects of LV-hGLB1 WT and OPT on the clonogenic capacity of human HSPCs. Results show the number and type of colony (white, granulocyte-macrophage colony-forming unit; red, burst-forming unit-erythroid; red dot, granulocyte, erythrocyte, monocyte, and megakaryocyte colony-forming unit). Values are expressed as median ± range. (B) Proliferation curve of human HSPCs transduced at different MOI (100, 30, 10) with LV-hGLB1 WT (left panel) and LV-hGLB1 OPT (right panel) expanded as myeloid liquid culture for 14 days. The proliferation capacity of UT cells was tested as a control. Values are reported as medians of log 10-fold increase compared with cell count at day 0 ± 95% confidence interval. (C) Single colony analysis of vector copy number (VCN). Each dot represents a colony. Median VCN ± range and percentage of positive colonies are reported for each condition. (D) ddPCR analysis of VCN integrated into the genome of the myeloid progeny of human HSPCs transduced with the LV-hGLB1 WT and LV-hGLB1 OPT. Values are reported as VCN median ± range. Any statistically significant differences were observed between the LV-hGLB1 WT and LV-hGLB1 OPT at MOI of 30 and 10. (E) Representative image of western blot analysis of β-GAL expression in the cell pellet and extracellular medium of the myeloid progeny of human HSPCs transduced with LV-hGLB1 WT and LV-hGLB1 OPT at different MOI (100, 30, 10). UT cells were used as controls. Actin-beta (ACTB) was used as a normalizer. β-GAL activity measured in the cell pellet (F) and conditioned medium (G) from the myeloid progeny of transduced HSPCs. Results are normalized on the amount of tested protein extract (mg) and conditioned medium (mL). Results show the enzymatic activity median ± range. Any statistically significant differences in the levels of β-GAL activity were observed between cells transduced with LV-hGLB1 WT and LV-hGLB1 OPT at an MOI of 30 and 10. Data were collected from three HSPC samples transduced at an MOI of 30 and 10, and from two HSPC samples transduced at an MOI of 100. Statistical analyses were conducted on samples transduced at an MOI of 30 and 10, compared with UT cells. *p* values were calculated using the Mann-Whitney test for all experiments.

The expression of human *GLB1* mRNA and β-GAL release are cell specific

We next investigated the reasons for impaired β-GAL release in the extracellular medium of transduced HSPCs. Along the multi-step processing of lysosomal enzymes, 5% to 10% of lysosomal proteins are released as precursors due to the leaking recognition system for lysosomal targeting mediated by mannose 6-phosphate receptor (M6PR) in the Golgi network.[33–36] Our data showed that the myeloid cells differentiated from transduced HSPCs failed to accumulate the

β-GAL precursor (84 kDa). On the contrary, compared with UT cells, we detected a robust expression of the lysosomal form of β-GAL (64 kDa) that is unavailable for cell secretion (Figure 1E). We found that the level of vector-derived *GLB1* mRNA expression was cell-type dependent, with the lowest level of mRNA in myeloid cells derived from the differentiation of LV-hGLB1 WT (LV-hGLB1) transduced HSPCs (Figure 2C). This result suggests that the *GLB1* expression levels may be insufficient in sustaining a robust protein production, thus preventing the accumulation of the enzyme precursor associated
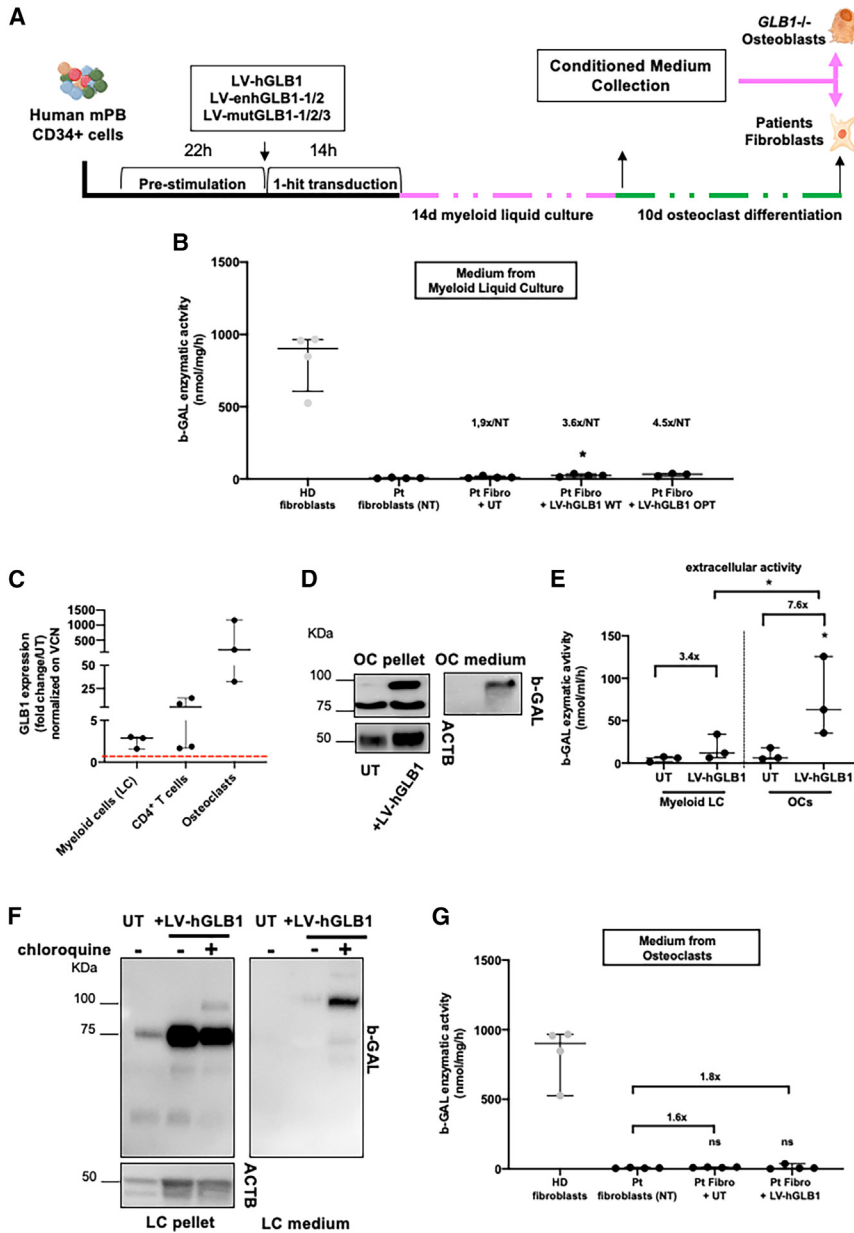
Figure 2. Analysis of β-GAL release from different cell types transduced with the LV-hGLB1

(A) Schematic representation of the cross-correction assay. We differentiated transduced HSPCs into myeloid cells for 14 days (pink lane). At the end of the differentiation, medium from myeloid cells is collected after 24 h conditioning. Myeloid cells are differentiated into osteoclasts (OCs) in the presence of receptor activator of nuclear factor kappa-B ligand (RANKL) and macrophage colony-stimulating factor (M-CSF) for 10 days (green lane). Medium from OCs was collected after 24 h conditioning. β-GAL-deficient cells are exposed for 12 h to the conditioned medium and collected for enzymatic activity measurement. (B) β-GAL activity measured in MPSIVB fibroblasts exposed to the conditioned medium from the myeloid liquid culture of human HSPCs untransduced (UT) or transduced with the LV-hGLB1 WT and LV-hGLB1 OPT. We used untreated patient fibroblasts (NT) and fibroblasts from healthy donor as controls. Results show the median enzymatic activity measured as nmol/mg/h ± range (n ≥ 3). (C) qPCR analysis of *GLB1* expression in different cell types transduced with the LV-hGLB1 WT (LV-hGLB1) at an MOI of 30. Results represent fold changes ($2^{\Delta\Delta CT}$) compared with UT cells. ΔΔCT = ΔCT transduced cells – ΔCT untransduced control. ΔCT = Ct GLB1 – Ct ACTB. Results are expressed as ΔΔCT median ± range (n ≥ 3). (D) Western blot analysis of β-GAL expression in the cell pellet and medium of OCs derived from the differentiation of UT and LV-hGLB1 WT (LV-hGLB1) transduced HSPCs. ACTB was used as sample normalizer. (E) β-GAL activity measured in the extracellular medium of myeloid cells (Myeloid LC) and OCs differentiated from human HSPCs transduced with LV-hGLB1 WT (LV-hGLB1) (MOI = 30). Results are expressed as β-GAL activity (nmol/h/mL) median ± range (n ≥ 3). Fold change compared with untransduced control cells are also reported. (F) Western blot analysis of β-GAL expression in the cell pellet and medium of myeloid cells transduced with LV-hGLB1 WT (LV-hGLB1) at an MOI of 30 treated (+) with 100 μM chloroquine to inhibit the intracellular lysosomal flux. Untreated (−) and untransduced myeloid cells were tested as controls. ACTB was used as sample normalizer. (G) Cross-correction assay of MPSIVB fibroblasts treated for 12 h with the conditioned medium from LV-hGLB1 WT (LV-hGLB1) and untransduced (+UT) OCs. Untreated patient cells (Pt fibroblasts NT) and fibroblasts from healthy donors (HD fibroblasts) were used as controls. Results show the median of β-GAL activity expressed as nmol/h/mL. Fold change of β-GAL activity on untreated cells are also reported. *p* values were determined by Mann-Whitney test for all the experiments. Bonferroni correction was applied in the case of multiple comparison (*$p < 0.05$, **$p < 0.01$).

with lysosomal trafficking overload. Consistent with our hypothesis, we observed the accumulation of β-GAL precursors in myeloid cell-derived osteoclasts (OCs) (Figures 2D, S1C, and S1D) and transduced CD4⁺ T cells (Figures S1E and S1F) expressing higher levels of *GLB1* mRNA compared with myeloid cells (Figure 2C). The superior accumulation of enzyme precursor available for cell release correlated with increased β-GAL activity in the cell supernatant of transduced OCs compared with myeloid cells (Figure 2E). Moreover, myeloid

cells accumulated the enzyme precursor in the cell pellet and released β-GAL in the extracellular medium upon treatment with chloroquine (100 μM), which is known to inhibit the lysosomal enzyme processing causing the accumulation of undigested enzyme precursor[36–38] (Figure 2F). We obtained similar results upon 24-h treatment with the lysosomal hydrolase inhibitor bafilomycine A1 (Figure S2A). Based on this evidence, we attempted to enhance β-GAL expression in myeloid cells by adding the eIF4A sequence (LV-eIF4A-hGLB1),
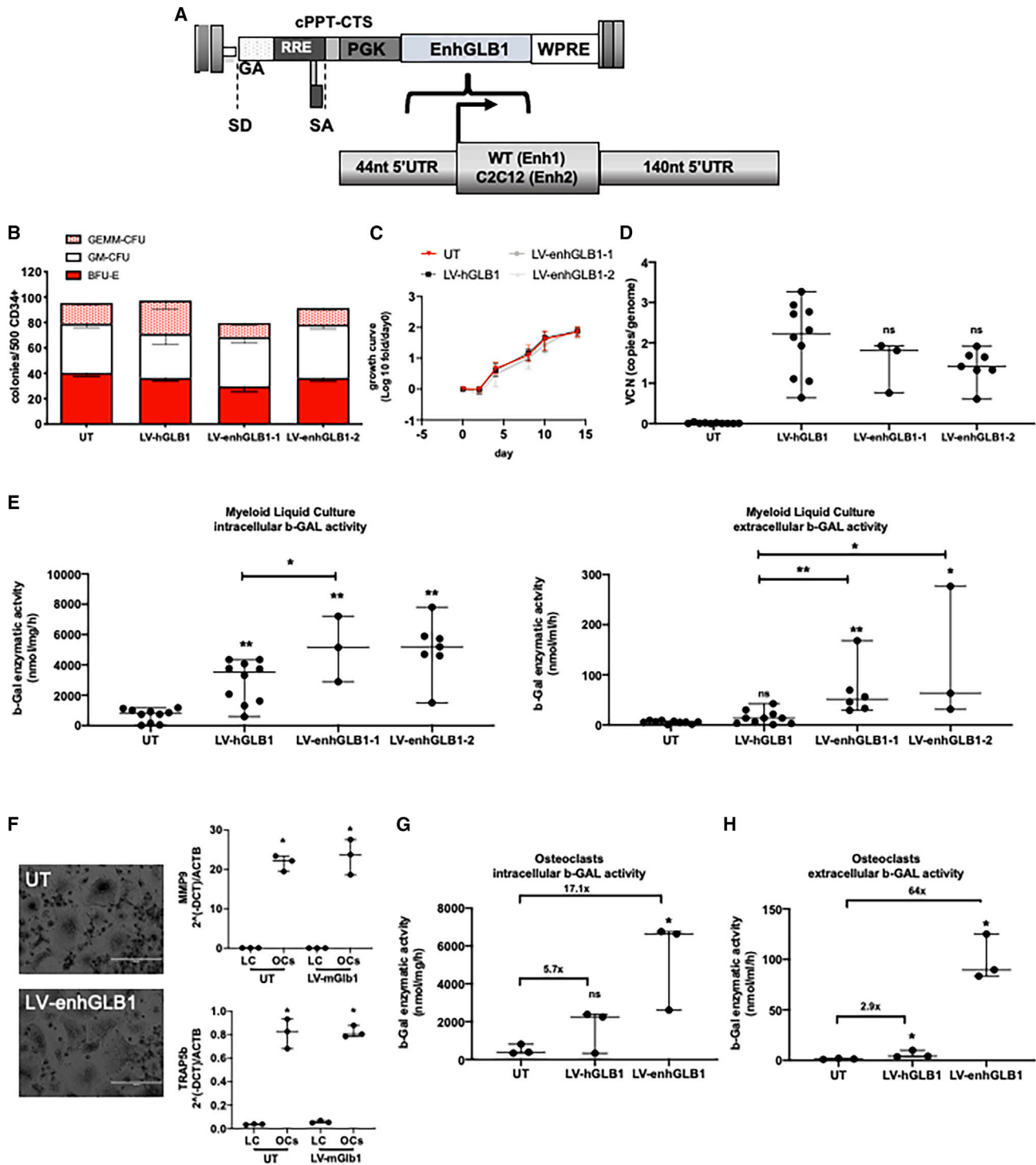
Figure 3. *In vitro* testing of lentiviral vectors encoding for the enhanced β-GAL

(A) Schematic representation of the lentiviral transfer vector encoding the enhanced β-GAL deriving from murine wild-type (LV-enhGLB1-1) and C2C12 GLB1 (LV-enhGLB1-2) cDNA. The transgene included the endogenous 5′ UTR (44 nucleotides upstream of the starting codon) and 3′ UTR (44 nucleotides downstream of the stop codon). (B) Clonogenic capacity of human HSCPs transduced with the LV-enhGLB1-1 and LV-enhGLB1-2 (MOI of 30). Results are expressed as the colony number and type median ± range ($n \geq 3$). Untransduced cells and HSPCs transduced with LV-hGLB1 (MOI of 30) were analyzed as controls. (C) Growth curve of untransduced and transduced HSPCs (MOI of 30) expanded as myeloid liquid culture for 14 days. (D) ddPCR analysis of VCN integrated into the genome of myeloid cells transduced with the different lentiviral

(legend continued on next page)

known to facilitate the initiation complex formation for RNA translation,[39] upstream of the *GLB1* cassette (Figure S3A). Although we successfully increased GLB1 expression in HEK293T cells (Figure S3B), there was no significant effect on enzyme accumulation and release using the LV-eIF4A-hGLB1 in myeloid cells (Figures S3C and S3D), suggesting that a cell-specific expression of *GLB1* mRNA could impact the release of β-GAL. Nevertheless, also the medium conditioned by transduced OCs failed to cross-correct MPSIVB fibroblasts despite the relatively higher *GLB1* mRNA expression and higher β-GAL activity (Figures 2C and 2G).

Taken together, these data pointed to a potential role of the human β-GAL stability, which rapidly diminishes at physiological temperature upon release.[13,40,41] Indeed, our *in vitro* studies showed that the human recombinant β-GAL had lower specific activity compared with the murine recombinant enzyme (70-fold), confirming the reduced stability of the human enzyme at 37°C and, thus, providing a rationale for the low β-GAL activity in the culture supernatants from transduced myeloid cells (Figure S4A). Importantly, while we could measure β-GAL activity in the plasma of C57BL6 wild-type mice, the plasma of pediatric healthy donors (*n* = 5) tested negative for β-GAL activity, indicating impaired functionality of human β-GAL in the extracellular space even at a physiological level (Figure S4B).

An enhanced *GLB1* transgene allows to reach supraphysiological levels of β-GAL in the extracellular medium of transduced human HSPCs inducing metabolic correction of diseased cells

Therefore, we considered the possibility of employing an enhanced *GLB1* transgene deriving from murine sequences to overcome the activity and release issues associated with the human transgene. We replaced the human *GLB1* cDNA with two different versions murine *GLB1* coding sequences: the wild-type (NM_009752.2, LV-enhGLB1-1) and the isoform expressed by the C2C12 cell line (LV-enhGLB1-2), characterized by three amino acid substitutions (Arg468Gln, Asn517Asp, and Glu534Gly) compared with the WT protein (Table S1; Figure S4C). We generated the respective LVs (LV-enhGLB1-1, LV-enhGLB1-2, and LV-hGLB1) (Figure 3A) to transduce mPB human HSPCs from healthy donors (Figure S1A). We did not observe signs of toxicity in transduced HSPCs clonogenic capacity and proliferation, meaning that the expression of the murine enzyme did not impact the number and composition of the HSPC colonies (Figures 3B and 3C). Human HSPCs were

efficiently transduced without significant differences in VCN (median VCN myeloid cells: LV-hGLB1 = 2.23, LV-enhGLB1-1 = 1.81, and LV-enhGLB1-2 = 1.4; Figure 3D). We then evaluated the levels of intracellular β-GAL expression and release in the culture supernatants from myeloid cells (Figure 3E). The expression of LV-derived murine β-GAL resulted in a higher median enzymatic activity (5,150 nmol/mg/h for LV-enhGLB1-1; 5,190 nmol/mg/h for LV-enhGLB1-2) compared with the expression of the LV-hGLB1 (3,522 nmol/mg/h for LV-hGLB1), leading to 6.3- and 4.3-fold increase in β-GAL activity compared with UT cells using the LV-enhGLB1 (1 and 2) and the LV-hGLB1, respectively (Figure 3E, left panel). These results were in line with previous works showing the dependence of the human β-GAL intracellular activity on the formation of a protein protective complex.[13,42] Importantly, we detected a significantly higher level of enzymatic activity in the CM from myeloid cells derived from the differentiation of human HSPCs transduced with LV-enhGLB1 (median β-GAL activity: 51 nmol/mg/h for LV-enhGLB1-1; 63 nmol/mg/h for LV-enhGLB1-2), corresponding to 8.2-fold (LV-enhGLB1-1) and 10.2-fold (LV-enhGLB1-2) increase of median enzymatic activity compared with UT cells. On the contrary, enzymatic activity in LV-hGLB1 transduced cells (median: 14 nmol/mg/h) did not increase significantly (Figure 3E, right panel). We further differentiated transduced myeloid cells into OCs and found that LV-enhGLB1-1 (LV-enhGLB1) transduced cells differentiated into tartrate-resistant acid phosphatase (TRAP)-positive OCs overexpressing MMP9 and TRAP5b, similarly to UT (Figure 3F) and LV-hGLB1 transduced myeloid cells (Figures S1C and S1D). We measured a 64-median fold higher β-GAL activity in the OC medium deriving from myeloid cells transduced with the LV-enhGLB1 compared with UT OCs. This increase was approximately 20 times higher than that observed in OCs transduced with LV-hGLB1 (Figures 3G and 3H). Thus, the use of LV-enhGLB1, either bearing the native murine cDNA or the C2C12 isoform, allowed turning human HSPCs into circulating (myeloid cells) and skeletal tissue-resident (OCs) cells capable of releasing supraphysiological levels of β-GAL that could potentially mediate the cross-correction of diseased cells.

To further confirm the therapeutic relevance of the LV-enhGLB1 constructs, we developed a 2D cell system using the HS5 stromal cell line to mimic the cross-correction of skeletal cells *in vitro*. We generated *GLB1*−/− HS5 stromal cells by CRISPR-Cas9 technology, using CRISPR mock HS5 cells as controls. *GLB1*−/− HS5

vectors. Results are expressed as VCN median ± range. (E) β-GAL activity measured in the cell pellet (nmol/mg/h) and extracellular medium (nmol/mL/h) of the myeloid progeny of human HSPCs transduced with LV-hGLB1, LV-enhGLB1-1, and LV-enhGLB1-2 at an MOI of 30. Untransduced cells were used as controls. Results are expressed as median enzymatic activity ± range. Each dot represents a biological replicate. (F) Representative image of tartrate-resistant acid phosphatase (TRAP) assay performed on the myeloid cells untransduced (UT) and transduced with the LV-enhGLB1-1 (LV-enhGLB1) (MOI = 30) after 10 days of differentiation into OCs. Scale bars, 100 μm (left panel). qPCR expression analysis of *MMP9* and *TRAP5b* as markers of OC differentiation in myeloid cells and OCs transduced with LV-enhGLB1-1 (LV-enhGLB1). UT cells were used as controls. Results are expressed as 2^(−ΔCT), and ΔCT is calculated as Ct gene – Ct ACTB. Results are expressed as median 2^(−ΔCT) ± range (*n* ≥ 3). β-GAL activity in the cell pellet (G) and extracellular medium (H) of OCs derived from the differentiation of human HSPCs transduced with the LV-hGLB1 and LV-enhGLB1-1 (LV-enhGLB1) (MOI = 30). Results are expressed as enzymatic activity median ± range (*n* ≥ 3). *p* values were determined by Mann-Whitney test for all the experiments. Bonferroni correction was applied in the case of multiple comparison (**p* < 0.05, ***p* < 0.01).
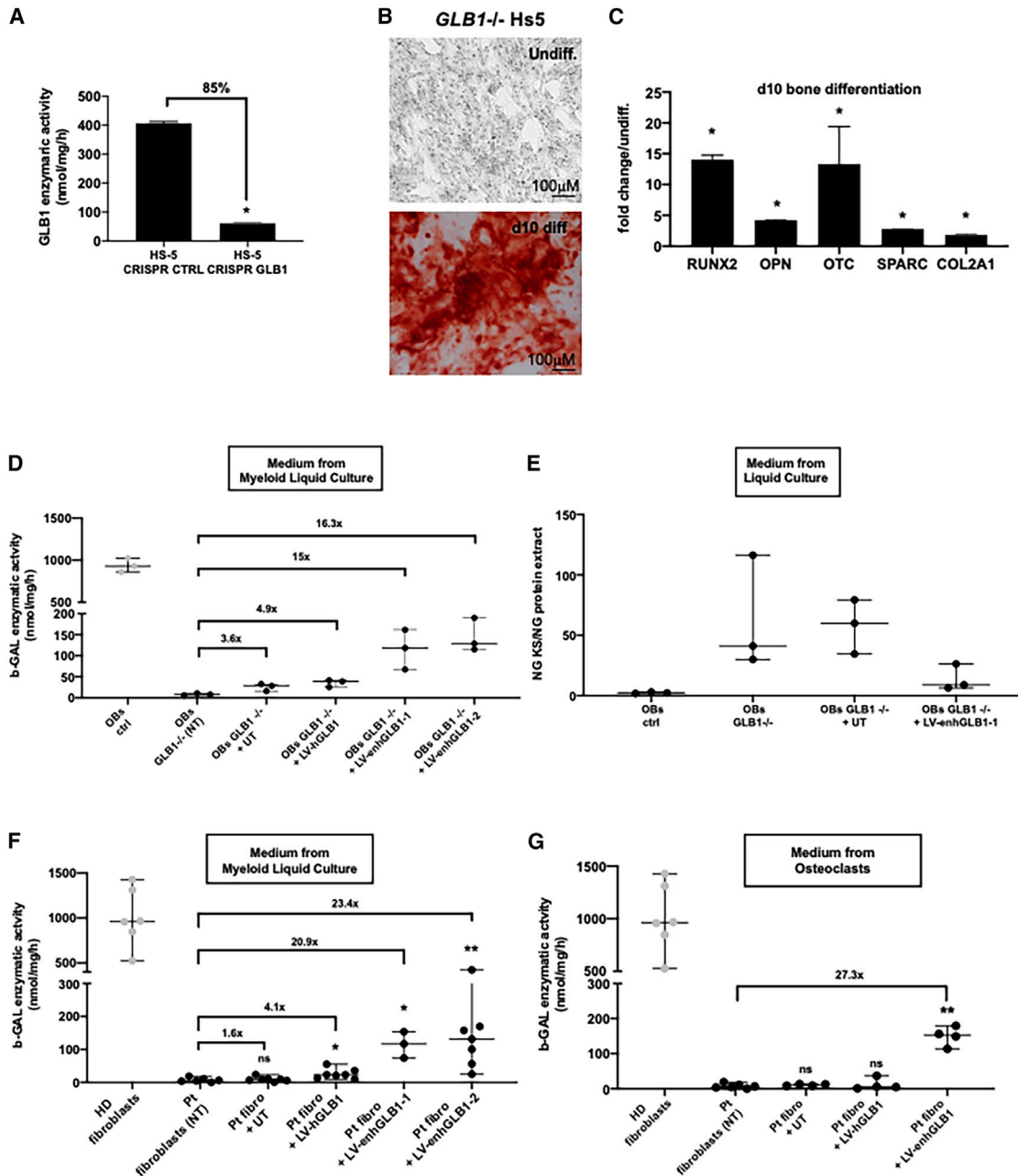
Figure 4. *In vitro* cross-correction of β-GAL-deficient cells

(A) β-GAL activity measured in HS5 stromal cells transduced with a lentiviral vector to abolish GLB1 expression by CRISPR-Cas9 technology. HS5 stromal cells transduced with a lentiviral vector bearing a control gRNA were used as controls. Data were collected from three independent measurement. Results show the median level of enzymatic activity normalized for the protein content (nmol/mg/h) ± range ($n \geq 3$). The percentage of β-GAL activity reduction is also reported. (B) Representative image of alizarin red staining performed on GLB1−/− HS5 cells induced to differentiate into osteoblasts for 10 days in proper medium. Undifferentiated cells were used as control. (C) qPCR expression analysis of skeletal differentiation genes. Data were collected from three independent assay of osteogenic differentiation. Results are expressed as median ΔΔCT on undifferentiated cells ± range ($n \geq 3$). ΔCT was calculated as Ct gene – Ct ACTB. (D) β-GAL activity in osteoblasts (OBs) (GLB1−/−) derived from the differentiation of GLB1−/− HS5 stromal cells upon 12-h treatment with the conditioned medium from untransduced myeloid cells (+UT) and from myeloid cells transduced with LV-hGLB1 (LV-GLB1), LV-enhGLB1-1, and LV-enhGLB1-2 at an MOI of 30. Untreated GLB1−/− OBs (NT) and control OBs were used as controls. Data were collected from three independent assay of osteogenic differentiation for control and GLB1−/− OBs. The level of β-GAL activity was measure on GLB1−/− OBs exposed to the cell supernatant of myeloid cells deriving from three different independent HSPC transduction experiments. Results show the median level of enzymatic activity normalized for the protein content (nmol/mg/h) ± range ($n \geq 3$). (E) Level of keratan sulfate (KS) measured by ELISA assay in the pellet of GLB1−/− OBs treated with the conditioned medium from

(legend continued on next page)

cells displayed 85% reduction in β-GAL activity compared with control cells (Figure 4A) and properly turned into osteoblasts (OBs) positive for alizarin red staining, activating the expression of skeletal differentiation markers (Figures 4B and 4C). We treated GLB1−/− OBs for 12 h with the CM from myeloid cells transduced with the different LVs. CRISPR mock (ctrl) and untreated GLB1−/− OBs were used as controls. β-GAL activity was restored at higher levels upon incubation with the CM from LV-enhGLB1 transduced cells (median fold change over untreated OBs (NT) = 15 for LV-enhGLB1-1 and 16.3 for LV-enhGLB1-2) (Figure 4D). On the contrary, the CM from LV-hGLB1 cells partially cross-corrected GLB1−/− OBs (median fold change over untreated OBs (NT) = 4.9), reaching an enzymatic activity similar to that induced by the CM from UT cells (Figure 4D). We further evaluated the accumulation of KS in skeletal cells by ELISA. We found a trend of KS reduction in GLB1−/− HS5 cells exposed to the CM from LV-enhGLB1-1 myeloid cells (Figure 4E). To confirm our data, we treated MPSIVB fibroblasts for 12 h with the CM from UT and transduced myeloid cells (Figures 4F and 4G). As expected, the level of β-GAL in patients' cells treated with the medium conditioned by UT cells was similar to that of untreated MPSIVB fibroblasts (NT). The CM from LV-hGLB1 transduced cells partially restored the β-GAL activity (median fold change to untreated fibroblasts = 4.1). We observed a statistically significant increase of β-GAL activity in patient cells treated with the cell supernatants of myeloid cells transduced with the LV-enhGLB1-1 and LV-enhGLB1-2 (median fold change to untreated MPSIVB fibroblasts: 20.9 and 23.4 for LV-enhGLB1-1 and LV-enhGLB1-2, respectively) (Figure 4F). The LV-enhGLB1 allowed to reach a statistically significantly improvement of β-GAL activity than the LV-hGLB1 in patients fibroblasts ($p = 0.05$ for LV-enhGLB1; $p = 0.0072$ for LV-enhGLB1). We obtained similar results when we treated MPSIVB fibroblasts with the cell supernatants from OCs derived from the differentiation of myeloid cells transduced with the LV-enhGLB1-1 (LV-enhGLB1) (median fold change to untreated MPSIVB fibroblasts: 27.3) (Figure 4G). Despite detecting the human enzyme in the cell supernatants of LV-hGLB1 transduced OCs (Figure 2D), this treatment failed to induce metabolic correction of MPSIVB fibroblasts (Figure 4G).

Our *in vitro* results demonstrated that human HSPCs overexpressing the murine enzyme generated myeloid cells/OCs releasing supraphysiological levels of β-GAL enzyme, which was efficiently uptaken by diseased cells (GLB1 KO HS5-derived OBs and patients' fibroblasts). Altogether, our results sustained the use of the LV encoding for the enhanced β-GAL for the preclinical development of HSPC-GT for MPSIVB.

β-GAL activity was restored in HSPCs from Glb1−/− mice transduced with LV-enhGLB1

To test the feasibility of gene correction of murine HSPCs from Glb1−/− mice for future preclinical development of HSPC-GT for MPSIVB, we isolated lineage-negative cells (Lin−) from the bone marrow (BM) of 7-week-old Glb1−/− mice. Lin− cells were transduced at an MOI of 100 with the LV-hGLB1 and the two LV-enhGLB1, according to previous studies on murine cells.[43] UT cells were used as controls (Figure 5A). We tested the clonogenic potential by colony-forming unit (CFU) assay, showing for transduced cells a colony number and composition similar to UT controls (Figure 5B). All the colonies were transduced without statistically significant differences in the mean VCN (Figure 5D). Transduced murine HSPCs proliferated similarly to controls and showed similar VCN at the end of the liquid culture (Figures 5C and 5E). We measured the β-GAL activity intracellularly and in the extracellular medium conditioned for 24 h by transduced and control cells (Figures 5F and 5G). β-GAL activity was restored in transduced cells, which showed a median enzymatic activity of 3,766 and 2,576 nmol/h/mg when treated with LV-enhGLB1-1 and −2, respectively. Glb1−/− HSPCs transduced with LV-hGLB1 exhibited reduced levels of β-GAL activity (median: 597.2 nmol/h/mg) (Figure 5F, left panel). The LV-enhGLB1 allowed reaching superphysiological levels of β-GAL, with LV-enhGLB1-1 showing a 7.8-fold increase and LV-enhGLB1-2 showing a 5.1-fold increase in β-GAL activity compared with LV-hGLB1 (Figure 5F, right panel). These differences were more evident for the β-GAL activity measured in the extracellular medium of transduced cells (Figures 5F and 5G, right panels). The median enzymatic activity measured in the extracellular space was higher in Glb1−/− HSPCs transduced with LV-enhGLB1 (83.8 nmol/h/mg for LV-enhGLB1-1 and 74.9 nmol/h/mg for LV-enhGLB1-1) than in cells treated with LV-hGLB1 (14.6 nmol/h/mg) (Figure 5G, left panel). The median β-GAL activity normalized on the VCN was 18- and 17-fold higher in the CM from LV-enhGLB1 transduced Glb1−/−1 HSPCs compared with cells treated with LV-hGLB1 (Figure 5G, right panel). These data further confirmed the feasibility of LV-enhGLB1 correction and the absence of toxicity also in the murine setting.

Human HSPCs overexpressing the enhanced β-GAL engraft and differentiate properly in humanized mice

To exclude any potential negative impact on the engraftment and reconstitution capacity of human cells overexpressing the murine

---

untransduced myeloid cells (+UT) and from myeloid cells transduced with LV-hGLB1 (LV-GLB1), LV-enhGLB1-1, and LV-enhGLB1-2 at an MOI of 30. Untreated GLB1−/− OBs (NT) and control OBs were used as controls. Results are expressed as ng of KS normalized for the amount (NG) of protein content. Each dot represents a biological replicate. Cross-correction assay performed on MPSIVB fibroblasts treated for 12 h with the conditioned medium from myeloid cells (F) transduced with the LV-hGLB1, LV-enhGLB1-1, and LV-enhGLB1-2 and OCs (G) transduced with the LV-hGLB1 and LV-enhGLB1-1 (LV-enhGLB1). The level of enzymatic activity was normalized on the amount of protein extract (mg). Patient fibroblast treated with the conditioned medium from UT cells were used as controls. Untreated patient cells (NT) and fibroblasts from healthy donors were used as reference. Results are expressed as the median β-GAL activity mean ± range ($n \geq 3$). Fold changes of median enzymatic activity compared with untreated MPSIVB fibroblasts are also reported. p values were determined by Mann-Whitney test for all the experiments. Bonferroni correction was applied in the case of multiple comparison (ns $p \geq 0.05$, *$p < 0.05$, **$p < 0.01$).
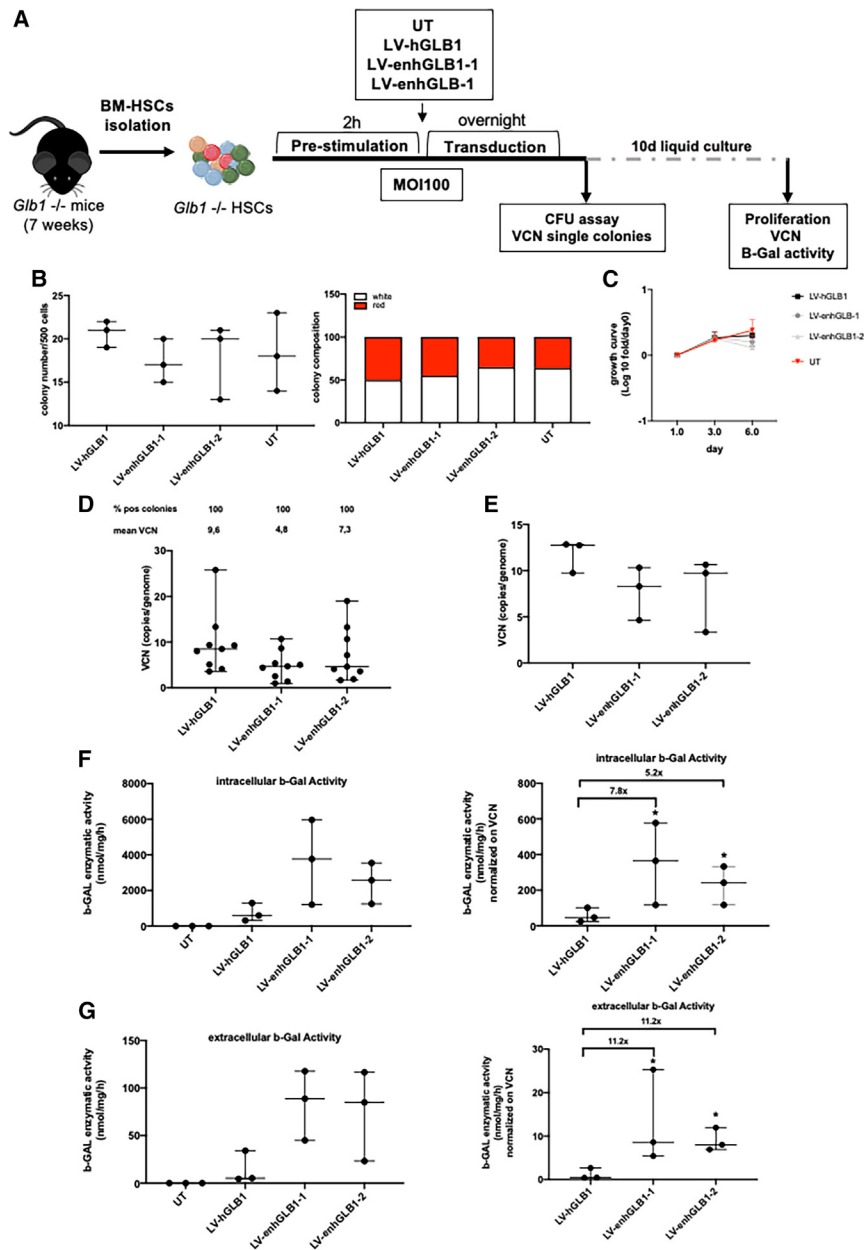
Figure 5. *In vitro* transduction of HSPCs from *Glb1−/−* mice

(A) Experimental scheme of isolation, purification and transduction of lineage negative (Lin−) HSPCs from *Glb1−/−* mice. (B) Number (left panel) and composition (right panel) of colonies formed by untransduced and transduced HSCs 14 days of culture in methylcellulose-based media. (C) Proliferation analysis of untransduced and transduced cells expanded as liquid culture. (D) Analysis of VCN at single colony level used to determine the percentage of transduced cells (VCN > 0.5). (E) VCN analysis in transduced HSPCs expanded for 14 days as liquid culture. (F) β-GAL activity measured intracellularly in untransduced and transduced HSPCs. Normalization of β-GAL activity on VCN is reported in the right panel. (G) β-GAL activity measured in the cell supernatant from in untransduced and transduced HSPCs. Normalization of β-GAL activity on VCN is reported in the right panel. Results show median ± range. Each dot represents a biological replicate. *p* values were determined by Mann-Whitney test and corrected by Bonferroni correction for multiple comparison (*$p < 0.05$, **$p < 0.01$).

β-GAL, we transplanted human HSPCs transduced *in vitro* at an MOI of 30 with the following LVs: LV-hGLB1, LV-enhGLB1-1, and LV-enhGLB1-2 in immunodeficient mice (NBSGW). As controls, NBSGW mice were transplanted with cultured UT cells (Figure S5A). We monitored the body weight of transplanted mice over time (Figure S5B) and evaluated the level of human engraftment as the percentage of human CD45+ cells (% hCD45) in the peripheral blood (PB) at 8 and 16 weeks after transplantation (Figure 6A). Engraftment of human CD45+ cells in the PB of mice transplanted with human HSPCs transduced with LV-enhGLB1 (1 and 2) was similar to mock transduced controls (Figure 6A) and slightly reduced in mice

transplanted with LV-hGLB1 transduced cells (Figure 6A). At 16 weeks, we detected a comparable human engraftment in the BM and spleen of transplanted mice compared with mice transplanted with UT cells (Figures 6B and S5C), demonstrating that the expression of the murine β-GAL did not impact the biodistribution of transplanted cells. In the BM of transplanted mice, we observed that human HSPCs transduced with the different LVs differentiated into myeloid, B, T, and NK cells at a similar level compared with UT cells (Figure 6C). We also measured a similar percentage of human hematopoietic stem cells (HSCs) (CD34+, CD38−) in the BM of transplanted mice, proving that the *in vitro* gene modification procedure did not alter the primitive HSC compartment (Figure 6D). Importantly, we detected a significantly higher level of β-GAL enzymatic activity in the BM of mice transplanted with LV-enhGLB1-1 and -2 transduced HSPCs (2.1- and 2.7-fold compared with mice transplanted with UT cells) compared with mice injected with LV-hGLB1 transduced HSPCs (1.4-fold compared with mice transplanted with UT cells) (Figure 6F) despite the higher VCN in the latter group (Figure 6E). These differences appeared more evident when the enzymatic activity was normalized to the VCN (Figure 6G). Altogether, these *in vivo* data showed the capacity of transduced human HSPCs to engraft and reconstitute the hematopoietic system of immunodeficient mice similarly to UT cells. Transplantation of human HSPCs transduced with the LV-enhGLB1 allowed to reach significantly higher levels of β-GAL activity without evidence of altered biodistribution *in vivo*.
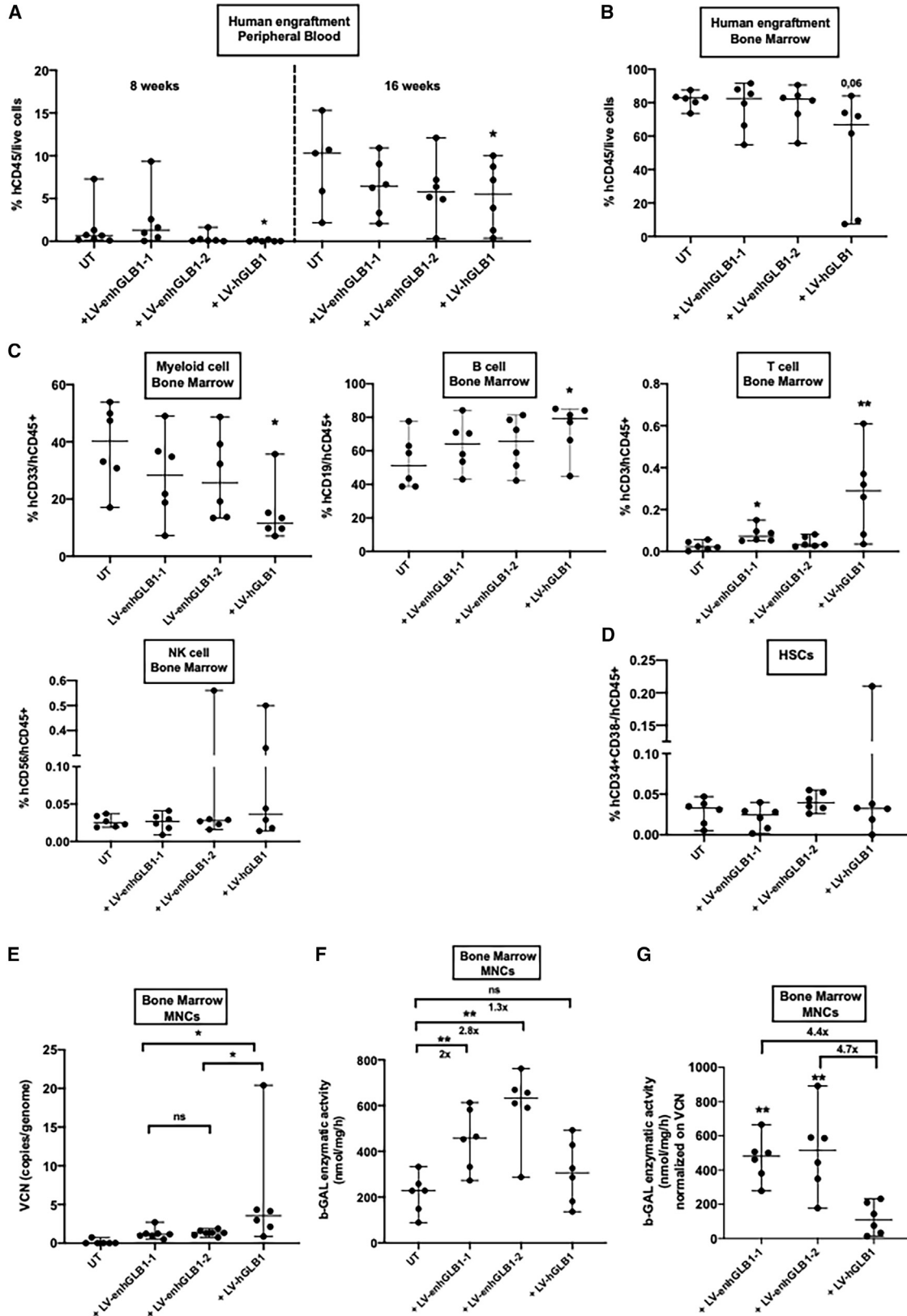
(legend on next page)

β-GAL trafficking and immunogenicity studies support the use of LV-enhGLB1 for HSPC-GT in MPSIVB patients

We next performed an additional study to support the use of the LV-enhGLB1 in the preclinical development of HSPC-GT and potentially in future clinical trials. The LV-enhGLB1-1 was chosen for further studies to avoid any theoretical concerns about the use of a *GLB1* isoform expressed by an immortalized cell line (C2C12). Considering that the metabolic correction mechanism in LSDs relies on the enzyme uptake from the extracellular environment and consequent lysosome targeting, we first performed a cross-correction assay in the presence of the natural M6PR ligand (M6P) to block the main pathway for lysosomal enzyme uptake (Figure S6A). We showed that M6P inhibited β-GAL uptake in patients' fibroblasts exposed to the CM from myeloid cell transduced with LV-enhGLB1, preventing their metabolic correction. We concluded that M6PR mediated the internalization of the murine similarly to the human enzyme (Figure S6A). We further evaluated whether the enhanced enzyme was directed toward the lysosomal compartment of human cells once internalized by immunofluorescence analysis of enhanced and human β-GAL, using β-GAL antibody in combination with the lysosomal marker LAMP-1 and vimentin to visualize the cell cytoplasm in MPSIVB fibroblasts (Figure S6B). We found that both the enhanced and human enzymes colocalized with LAMP1 in fibroblasts exposed to the CM from myeloid cells transduced with LV-enhGLB1 or LV-hGLB1. Fibroblasts exposed to the CM from UT cells were used as controls. Furthermore, we observed increased expression of LAMP1 in untreated and treated MPSIVB fibroblasts compared with healthy controls (Figures S6B and S2B). This increase may be associated with the compromised autophagy function described for other LSDs, preventing the effective degradation of engulfed lysosomes. Consequently, there is an accumulation of lysosomes in the diseased cells in contrast to the healthy controls.[44,45] Our results indicated that the murine enzyme was correctly targeted into the lysosomal compartment and colocalized with LAMP-1, similar to human β-GAL (Figure S6B). Importantly, higher amount of the murine β-GAL enzyme was internalized by patient cells. To provide deeper mechanistic insights about the higher cross-correction efficiency of the murine β-GAL, we performed a preliminary characterization of different endocytic trafficking pathways in healthy donor and patients' fibroblasts. We tracked receptor-mediated and fluid-phase endocytosis by analyzing the internalization of Alexa Fluor-conjugated BSA and dextran, respectively. Patients' fibroblasts displayed similar endocytic activity compared with healthy donors (Figures 7A and 7B). Furthermore, we studied the endosomal recycling pathway by measuring the recycling rate of fluorescently labeled transferrin that was efficiently uptaken and recycled by both healthy donor and patients' fibroblasts (Figure 7C). Next, we analyzed the involvement of the M6PR endocytic pathway, mostly responsible for the uptake and delivery of lysosomal enzymes, in murine β-GAL trafficking. Interestingly, using a dynamic assay of M6PR-mediated endocytosis, we observed a significant delay of M6PR arrival at the *trans*-Golgi network in patients' fibroblasts. Indeed, in healthy donor fibroblasts M6PR is clustered in the perinuclear region (high perinuclear index) whereas in patient's fibroblasts the M6PR is dispersed in the cytosol (low perinuclear index) (Figure 7D). The latter observation was confirmed by an increase in the colocalization of M6PR with EEA1, a well-described marker of early endosomes, in patient's fibroblasts (Figure 7E). Despite the delay in the trafficking of M6PR, patient's fibroblasts are perfectly capable of internalizing different types of cargos, including the M6P-modified lysosomal enzyme. At this point we performed a time course endocytosis assay of human and murine recombinant β-GAL in patient's fibroblasts. Strikingly, the murine recombinant enzyme was internalized more efficiently than human β-GAL already at 15 min (Figure 7F). After 2 h-exposure, we observed a superior intracellular amount of murine compared with human recombinant β-GAL (Figure 7F).

We then compared the protein structure of the enhanced and human enzymes,[46,47] identifying a 70% homology in the amino acid sequence, with only few amino acid residues displaying highly different biochemical features, such as size and hydrophobicity, at the homologous positions (Figure S4D). Based on this analysis, we attempted to identify specific amino acid residues that confer improved functional stability to the enhanced enzyme in the extracellular environment compared with its human counterpart. Since both the enzymes function as dimers, we hypothesized that the functional stability of the enzyme could rely on the monomer-monomer binding strength. Therefore, we focused on the biochemical differences at the interaction surfaces between the enhanced and human enzyme, predicting a diminished binding strength of the monomer-monomer binding for the human enzyme compared with the murine counterpart. This reduction is likely attributable to the presence of amino acid residues with diminished biochemical compatibility at the dimer interaction surface. Specifically, we identified glutamine 605 (Gln605) and lysine 66 (Lys66) as putative amino acid residuals responsible for the reduced strength of the human monomer-monomer binding. Therefore, we reasoned that substituting Gln605 with arginine (Arg) and Lys66 with glutamate (Glu) could enhance the biochemical compatibility with the interacting residues present on the opposite surface. Accordingly, we generated mutated cDNA variants: (1) Gln605Arg (LV-mutGLB1-1), (2) Lys66Glu (LV-mutGLB1-2), and (3) Gln605Arg + Lys66Glu (LV-mutGLB1-3), which were cloned in

Figure 6. *In vivo* biodistribution study of human HSPCs overexpressing the human and murine β-GAL

Evaluation of human cell engraftment as the percentage of human CD45+ cells on live cells in the peripheral blood at 8 and 16 weeks (A) and in the bone marrow (B) at 16 weeks post-transplantation. (C) Evaluation of multilineage differentiation of human HSPCs in the bone marrow of transplanted mice 16 weeks after treatment. Results show the percentage of human CD33+ (myeloid lineage), CD19+ (B cell lineage), CD3+ (T cell lineage), and CD56+ (NK lineage) cells on live cells. (D) Percentage of human HSPCs identified as human CD34+ CD38neg cells in the bone marrow 16 weeks post-transplantation. (E) ddPCR analysis of VCN integrated into the genome of bone marrow mononuclear cells isolated from transplanted mice. (F) β-GAL activity measured in the bone marrow mononuclear cells. The enzymatic activity was normalized on the VCN (G). For all the experiments: results show median ± range, each dot represents a biological replicate. *p* values were determined by Mann-Whitney test (*$p < 0.05$, **$p < 0.001$).
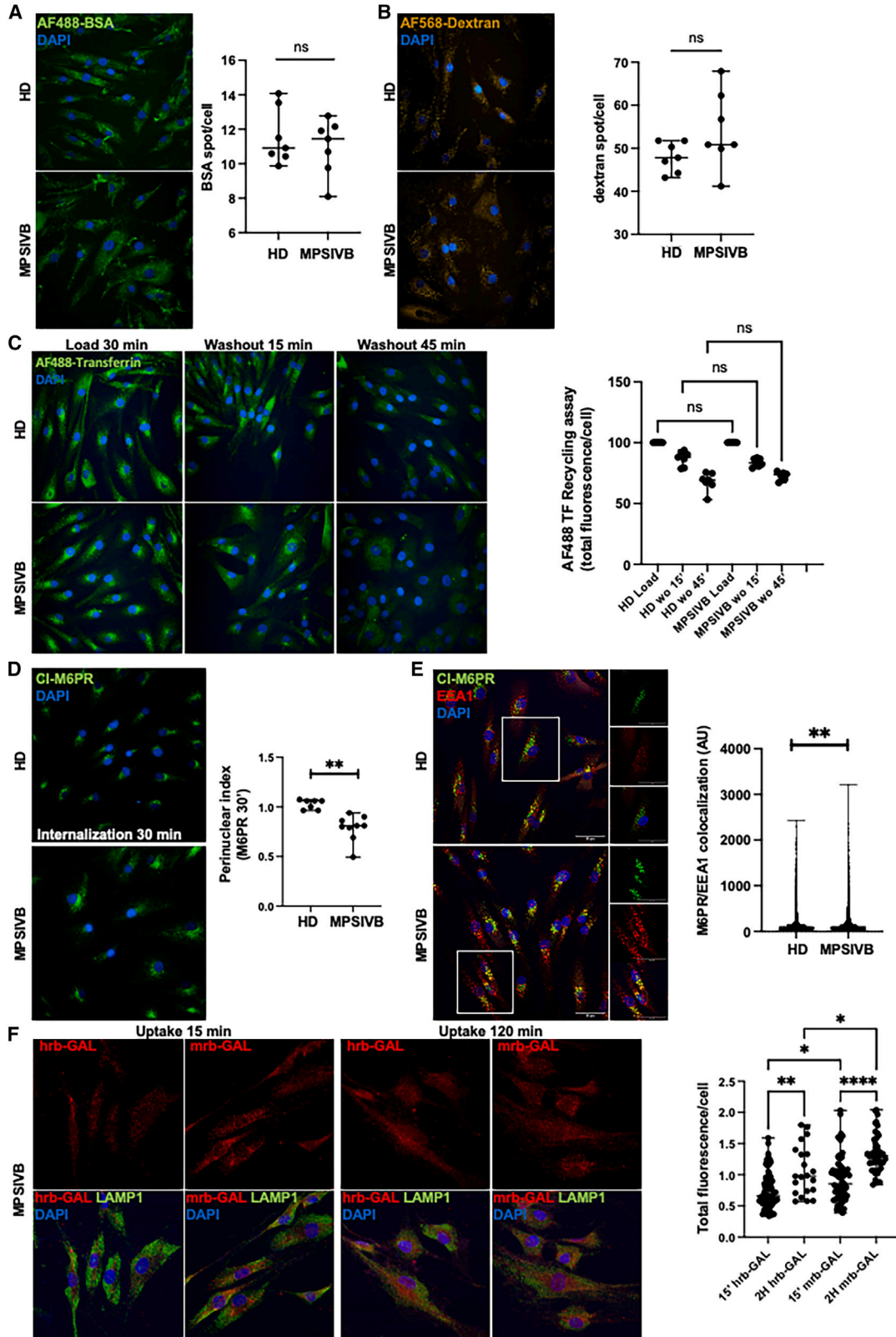
(legend on next page)

the same LV used for overexpressing the human and enhanced β-GAL in human HSPCs. HEK293T cells and human HSPCs were transduced with the newly generated LVs, using LV-hGLB1 and LV-enhGLB1 as controls. We found that the mutated transgenes were ineffective in inducing enzyme overexpression at supraphysiological levels in the cell supernatant and did not induce the metabolic correction of patient cells, mirroring the outcomes observed with the wild-type human GLB1 transgene (Figures S4E–S4G).

We further investigated the potential immunological risks associated with employing an LV encoding an enhanced enzyme of non-human origin for preclinical and future clinical development of HSPC-GT for MPSIVB patients. Indeed, the high sequence homology cannot warrant that the murine amino acid sequence would be devoid of immunogenicity in the context of the human immune system. To address concerns about possible xenogeneic immune reactions, we tested *in vitro* the primary and secondary response of PB mononuclear cells (PBMCs) from healthy donors to LV-enhGLB1-derived proteins (Figure 8). To this aim, the CM from HEK293T cells, either UT or transduced with LV-hGLB1, LV-enhGLB1-1, or LV-enhGLB1-2, was collected after 5 days of culture. The enzymatic activity of culture supernatants was measured, and β-GAL protein concentration was calculated based on recombinant enzyme titration curves (Figure S4A). PBMCs from healthy donors ($n = 2–5$) were cultured in the presence of CM at different dilution and we evaluated CD4+ T cell proliferation and IFN-γ production after 5 days (Figure 8A). While polyclonal stimulation with phytohemagglutinin (PHA) induced strong proliferation and IFN-γ release in all donors tested, stimulation with culture supernatants from transduced HEK293T cells did not elicit β-GAL-specific T cell response in any of the donors tested. To evaluate T cell response upon re-challenge, PBMCs from healthy subjects ($n = 3$) were cultured for 13 days in culture supernatants from UT, or LV-hGLB1/LV-enhGLB1 transduced HEK293T cells. In parallel, autologous CD14+ cells were isolated and differentiated into dendritic cells (DCs) in the presence of rh-IL-4 and rh-GM-CSF for 7 days and cryopreserved for subsequent T cell restimulation. After 13 days of culture, DCs were thawed and pulsed with the undiluted CM from UT HEK293T cells or transduced with LV-enhGLB1

(1 and 2) or tetanus toxoid (TT, control Ag), and used to restimulate the primary T cell cultures. While CD4+ T cell proliferation to polyclonal restimulation (PHA) and TT-specific response was detectable, specific response to enhanced β-GAL was absent in all donors tested (Figure 8B), indicating that the murine-derived enzyme sequence did not elicit significant T cell response, at least *in vitro*. We performed the same experiments on PBMCs from an MPSIVB patient and excluded an increased immunogenicity of the enhanced enzyme compared with the human counterpart also in patients (Figures S7A–S7C). Although the *in vitro* immunological tests cannot fully exclude the risk of an immune response against the murine-derived transgene in patients, our clinical experience demonstrated that a myelo- and lymphoablative preparative regimen before HSPC-GT favors immunological tolerance to the therapeutic enzyme also in patients previously treated with ERT.[25] Moreover, in null patients for β-GAL expression an immune response could be mounted in theory also against the human or the human engineered enzymes. Our analyses further support the use of LV-enhGLB1 for the preclinical development of HSPC-GT for MPSIVB and GM1-related disorders.

DISCUSSION

Based on the previous successful experiences in HSPC-GT for other LSDs,[25,28] in this work, we investigated the GLB1 transgene to optimize the production of a third-generation LV to overexpress β-GAL in human HSPCs for the future preclinical and clinical development of HSPC-GT for GM1-related disorders, who manifest severe skeletal and neurological symptoms. While no approved therapies are available for these patients, the preclinical data and ongoing experimental clinical trials of *in vivo* GT (NCT04713475, NCT03952637) target only the neurological manifestations of the disease through the AAV-mediated restoration of β-GAL expression in the brain of GM1-gangliosidosis patients.[48,49] On the contrary, our previous experience with MLD and MPSI-H has shown the safety and efficacy of HSPC-GT to induce beneficial effects on both the neurological and skeletal symptoms.[23–25,28,29] These findings suggest that gene-corrected HSPC progeny releases supraphysiological levels of the therapeutic enzyme, leading to improved targeting of barrier-protected

Figure 7. Characterization of intracellular trafficking pathways in healthy donor and patients' derived fibroblasts

Representative images and quantitative analysis of clathrin-mediated endocytosis of fluorescently labeled BSA (AF488-BSA, green) (A) and fluid phase endocytosis of fluorescently labeled dextran (AF568-dextran, orange) (B) in healthy donor (HD) and patients' (MPSIVB) fibroblasts. The number of AF488-BSA or AF568-dextran spots per cell was analyzed in more than 3,000 cells from three independent experimental replicates. (C) Recycling of transferrin receptor was tested in HD and MPSIVB fibroblasts upon incubation with 50 μg/mL of AF488-transferrin (green) for 30 min at 37°C (Loading phase). The AF488-transferrin was then washed out for 15 and 45 min in presence of 50 μg/mL of unlabeled transferrin to stimulate the recycling of transferrin receptor and the release of fluorescent transferrin. The intensity of intracellular AF488-transferrin was measured over time. The change (decrease) of the intensity is a proxy of the transferrin receptor recycling. The intensity of AF488-transferrin per cell was analyzed in more than 1,000 cells from three independent replicates. (D) The cation-independent M6PR trafficking was evaluated in HD and MSPIVB fibroblasts treated with 4 μg/mL of anti-M6PR mouse monoclonal antibody for 30 min. Cells were then fixed and subjected to immunofluorescence staining with anti-mouse AF488 antibody and nuclei were counterstained with DAPI. The quantitative analysis was performed on more than 1,000 cells from 3 independent replicates, dividing the cytoplasm of each cell in 2 regions (perinuclear and cell periphery). The graph reports the ratio of the fluorescence intensity of M6PR localized in the perinuclear region over the cell periphery. (E) Representative images and quantitative analysis of M6PR colocalization (green) with the early endosomal marker EEA1 (red). (F) Evaluation of human (hrGLB1) and murine recombinant β-GAL (mrGLB1) uptake in patients' fibroblasts upon treatment with the same amount of recombinant enzymes for 15 min and 2 h. After treatment, cells were stained with anti-β-GAL (red) and anti-LAM1 (green). Nuclei were counterstained with DAPI. Human or murine β-GAL fluorescence intensity was measured in at least 150 cells from 3 independent experiments and normalized over LAMP1 fluorescence intensity. For all the experiments: results are expressed as median ± range. p values were determined by Mann-Whitney test and Bonferroni correction in the case of multiple comparison (*$p < 0.05$, **$p < 0.01$, ***$p < 0.001$, ****$p < 0.0001$).
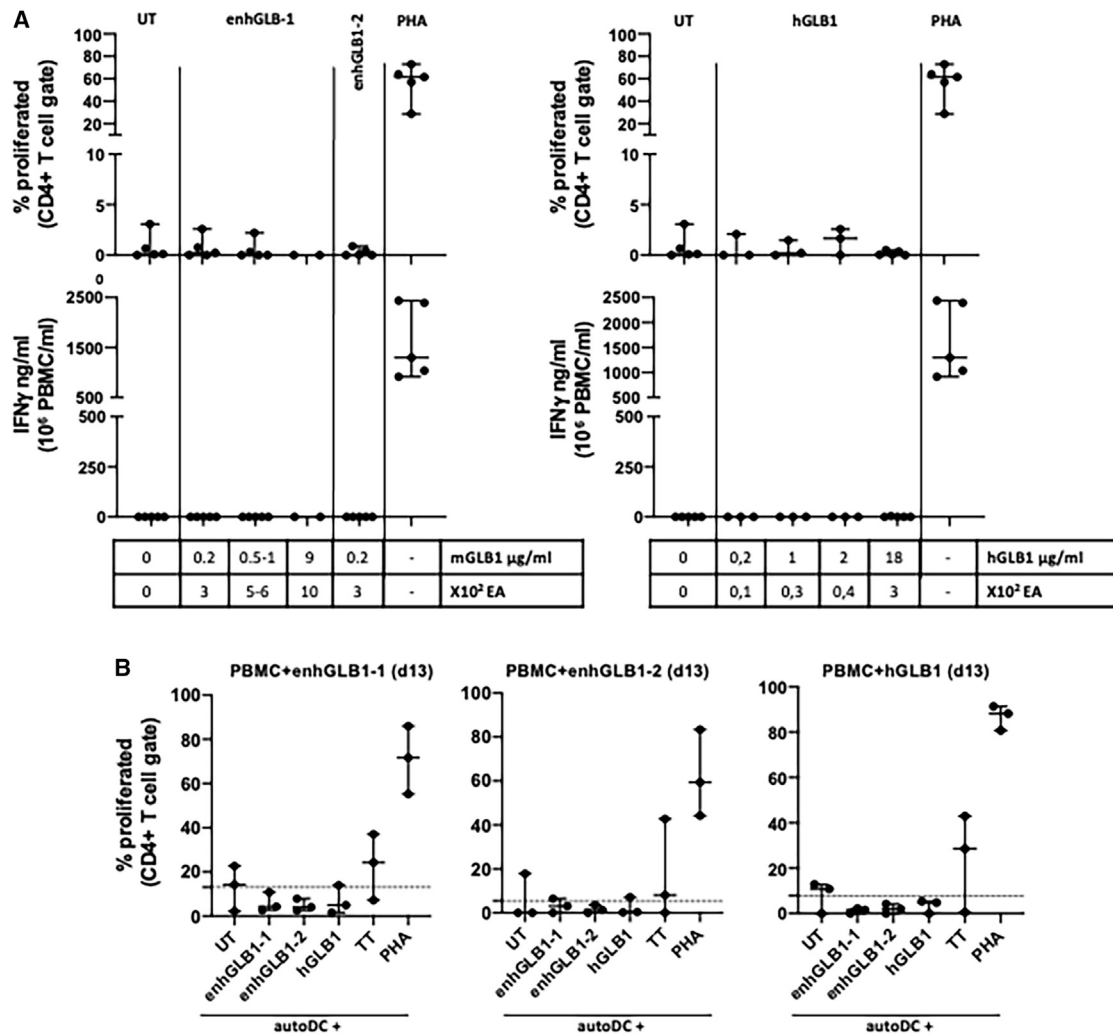
Figure 8. Evaluation of β-GAL immunogenicity

(A) PBMCs from healthy donors were cultured in the presence of increasing dilutions of the conditioned medium from HEK293T cells transduced with LV-enhGLB1-1, LV-enhGLB1-2 (left panels), and LV-hGLB1 (right panels). Vector-derived GLB1 protein content was estimated based on the titration curve of rmGLB1 and rhGLB1 enzymatic activity (EA) (Figure S4A). The T cell response was evaluated as CD4+ T cell proliferation (upper panels) and IFN-γ production (lower panels) after 5 days of exposure to the conditioned media. (B) Recall response to enhanced and human β-GAL was evaluated after *in vitro* restimulation of PBMC exposed for 13 days to the conditioned medium from HEK293T cells transduced with LV-enhGLB1-1 (left), LV-enhGLB1-2 (middle), and LV-hGLB1 (right). T cells were plated with pulsed autologous dendritic cells (DCs) at a 10:1 ratio and proliferation was evaluated after 3 days. Background proliferation to upulsed DCs was subtracted. Results are expressed as median ± range, each dot represents an independent healthy donor.

and poorly vascularized tissues. Indeed, sustained levels of the therapeutic enzyme were detected in the cerebrospinal fluid of HSPC-GT-treated patients,[25,28] resulting in a complete correction of the disease neurological manifestation, which are resistant to correction by HSCT. Given the similar clinical and pathogenetic characteristics of LSDs, we believe that this correction mechanism could also be effective for GLB1-related disorders. For the preclinical testing of HSPC-GT, we developed LVs bearing the wild-type and codon-optimized human *GLB1* transgenes and tested their toxicity and efficacy in human HSPCs from healthy donors, with the purpose of inducing a supraphysiological release of β-GAL from the progeny of transduced

HSPCs. We transduced mobilized human HSPCs representing a clinically relevant source of CD34+ cells for HSPC-GT in pediatric patients. We did not observe any toxic effects in terms of clonogenic capacity and cell proliferation using both vectors at transduction conditions under which intracellular transgene expression reached saturation. The codon-optimized transgene induced protein expression at a similar level to the wild type in the myeloid progeny of transduced HSPCs. Unexpectedly, we found that transduced HSPCs failed to release human β-GAL by WB and enzymatic activity, and the culture supernatants from transduced cells failed to restore β-GAL activity in patients' cells. In agreement with these data, when LV-hGLB1 WT

HSPCs were xenotransplanted in NBSGW mice, cells engrafted and differentiated but did not induce β-GAL overexpression. These data suggest that the LV-hGLB1 transgene is not suitable for the development of an HSPC-GT approach based on enzyme overexpression and consequent augmented cross-correction.

The PGK promoter has an excellent safety record in preclinical and clinical studies in the context of LV-based HSPC-GT.[26] It has been previously employed to drive ARSA and IDUA expression[50] in HSPCs and their myeloid progeny resulting in intracellular overexpression and enzyme release.[25,28] Indeed, the PGK expression is significantly active in the myeloid-monocyte compartment as indicated by the Human Protein Atlas immune cell dataset. The findings that human *GLB1* mRNA was lower in myeloid differentiated transduced cells than in OCs and T cells suggested a cell-type-dependent regulation of PGK-driven gene expression. We obtained similar results when we differentiated LV-PGK-IDUA transduced HSPCs into OCs, which showed higher enzymatic activity than myeloid cells (data not shown). Even if alternative stronger promoters might be considered to improve human *GLB1* mRNA expression, this choice must be balanced with the potential increased risk of insertional mutagenesis, as observed in X-ALD HSPC-GT.[51] Moreover, previous data from our Institute show that the integration site is primarily influenced by the LV backbone, regardless of the specific transgene incorporated. In our study, we used the same LV backbone as the MLD and MPSI-H clinical trials. Analysis of the PB and BM samples of MLD and MPSI-H patients who underwent HSPC-GT showed a stable and highly polyclonal repertoire, with no dominant clones or significant enrichment for oncogenes or tumor-suppressor genes.[25,28] These findings are consistent with integration profiling data obtained from other studies of LV-based GT.[23,52,53] Therefore, we believe that the risk of genotoxicity of LV-enhGLB1 is extremely low. The addition of the eIF4a sequence upstream of the start codon to stabilize the formation of the translation complex did not confer any advantages in terms of protein release in hematopoietic cells. Importantly, we found a link between the level of mRNA and the accumulation of enzyme precursors. The low amount of mRNA correlated with a low amount of protein precursor, efficiently processed into the lysosome, preventing the engulfment of the lysosomal protein trafficking. This overload was necessary for precursor accumulation and release. Altogether, these results highlighted a cell-specific stability of the *GLB1* mRNA and regulation of its expression contributing to the impaired β-GAL release from myeloid cells. A poor stability of the human β-GAL at 37°C[13] could also negatively impact the therapeutic use of the human enzyme, since also the CM from LV-hGLB1 transduced OCs, failed to restore β-GAL in patients' fibroblasts, despite OCs releasing the enzyme precursor. Previous works demonstrated that both the human and murine enzymes function as dimers,[46,47] and we predicted a stronger monomer-monomer binding for the murine dimer, possibly due to the presence of amino acid residues more biochemically compatible at the interaction surface. This binding strength could eventually explain the higher stability of the murine enzyme in the extracellular environment compared with the human counterpart. We conclude that the cell-dependent mRNA levels and

the thermal instability of the human β-GAL enzyme represent major hurdles to the further development of HSPC-GT. When the human *GLB1* transgene was selectively mutated to improve the biochemical compatibility of amino acid residues at the dimer interaction surface, we found that the mutated transgenes were ineffective in inducing supraphysiological expression of the therapeutic enzyme in the cell supernatant, preventing the metabolic correction of patient cells. Exploring alternative strategies, such as redesigning the human *GLB1* transgene through random mutagenesis techniques could potentially address these challenges. However, we reasoned that the murine enzyme is an evolutionary selected protein, with known function and effects. In contrast, *de novo* engineered proteins may introduce unpredictable adverse functions and likewise pose immunological risks.

Since the murine form of β-GAL is more stable[13–15] and has a higher enzymatic activity compared with the human recombinant enzyme, we designed an LV to overexpress an enhanced β-GAL deriving from murine sequences (LV-enhGLB1) in human HPSCs. We did not observe alterations in the clonogenic capacity, proliferation, differentiation into OCs, engraftment, and *in vivo* differentiation of LV-enhGLB1 transduced HPSCs. In the presence of similar VCN, myeloid cells showed significantly higher enzymatic activity when transduced with the LV-enhGLB1, achieving β-GAL overexpression in the extracellular medium of both transduced myeloid cells and OCs. Only cell supernatants from LV-enhGLB1 transduced myeloid cells and OCs achieved correction of MPSIVB patients' fibroblasts. We further compared the two LVs in a skeletal cell system, which is more relevant for predicting their therapeutic potential, and we demonstrated the restoration of the β-GAL activity in β-GAL-deficient OBs after treatment with the cell supernatants from myeloid cells transduced with LV-enhGLB1. In this setting, we also observed a trend of KS reduction, suggesting that the enhanced enzyme properly functioned in human cells. *In vivo*, we found a significantly higher β-GAL activity in mice transplanted with human HPSCs overexpressing the enhanced enzyme. Based on these data, we propose the use of LV-enhGLB1 for the preclinical development of HSPC-GT strategies for MPSIVB. Preliminary tests on murine HSPCs from the BM of *Glb1−/−* mice showed overexpression and increased β-GAL release from LV-enhGLB1 transduced cells compared with UT controls. We further investigated whether differences between the human and enhanced enzymes could prevent the use of LV-enhGLB1 in patients. First, we evaluated the trafficking of the enhanced β-GAL in patient fibroblasts, showing that the enhanced enzyme was internalized through the M6PR as efficiently as the human β-GAL. Moreover, the enhanced enzyme was correctly targeted into the lysosomal compartment, as shown by colocalization with the lysosomal marker LAMP1. No critical alterations were observed in the major endocytosis pathways in patients compared with healthy donor fibroblasts. In cross-correction assay, patients cells internalized more efficiently the enhanced β-GAL, measured as increased level of total intracellular enzyme at different time points post-treatment, which may show a superior affinity of the enhanced β-GAL to the human M6PR and/or the combined use of alternative endocytic pathways. Finally, we

addressed the potential immunological concerns on the enhanced enzyme overexpression in patients' cells. Previous preclinical work showed that anti-transgene T cell immunity could impact on HSPC-GT efficacy in immunocompetent hosts.[54] We therefore tested the immunogenicity of the human and enhanced enzymes using T cells from healthy donors challenged with the CM from HEK293T transduced with the LV-hGLB1 and LV-enhGLB1 at matched MOI. We did not find any differences in T cell response neither in primary stimulation nor at re-challenge, suggesting that the use of the enhanced β-GAL sequence is not expected to pose additional risks to those related to the administration of a human enzyme in patients lacking the β-GAL. These results were confirmed using T cells from a single MPSIVB patient. In any case, we have shown that the risk of developing an immune response against the transgene is substantially mitigated in the context of an autologous HSPC-GT when patients receive a myelo- and lymphoablative preparative regimen, as demonstrated in MPSI-H patients.[25] Moreover, the preclinical data of *in vivo* GT with an AAV9 carrying the murine GLB1 transgene demonstrate a phenotypic amelioration and extension in lifespan of treated GM1 mice.[49] These findings further support the clinical feasibility of our approach. In addition, when considering the cardiac defects associated with impaired elastinogenesis in MPSIVB patients due to mutations in the *GLB1* genetic regions common to EBP, the use of the murine-derived transgene does not pose a significantly higher risk of failing to address these symptoms. In fact, the LV can accommodate the cDNA sequence without the intronic regions involved in the alternative splicing responsible for EBP production.[55–57]

In conclusion, our study has generated preliminary proof-of-concept data, both *in vitro* and *in vivo*, to complete the preclinical development of HSPC-GT based on the LV-enhGLB1 in a mouse model of β-GAL deficiency, which exhibits mild signs of skeletal disease and severe neurological alterations.[29] Our initial data on murine HSPCs from *Glb1–/–* mice demonstrated supraphysiological levels of β-GAL enzyme in the progeny of HSPCs transduced with LV-enhGLB1 (Figure S7) without any observed toxicity *in vitro*. This result is consistent with our previous findings for MLD- and MPSI-H-derived murine HSPCs, suggesting a similar potential for correction upon transplantation. Our previous experience with MLD and MPSI-H mouse models demonstrated that *ex vivo* gene-corrected HSPCs generate hematopoietic tissue-resident cells, including CNS macrophage and microglia-like cells.[24,58] Similarly, OCs may represent a tissue-resident source of hematopoietic origin within the skeleton. The HSPC progeny leads to supraphysiological levels of the therapeutic enzyme in the CNS of treated mice, resulting in a complete correction of the neurological manifestation in these diseases, and significant amelioration of the skeletal alterations which are resistant to correction by HSCT. For the proof-of-concept study using the LV-enhGLB1 planned for the clinical translation of this project, we will follow the same approach (LV backbone, transduction protocol, and conditioning regime) that was successfully used in the preclinical studies in MLD and MSPI-H mouse models. We believe that this approach will ensures the local production of β-GAL, likely leading to an improvement of neurological symptoms in the *Glb1–/–* mouse model.

Our ultimate objective is to progress toward a clinical trial of HSPC-GT, aiming to address the urgent need for innovative and curative therapies for MPSIVB and GM1 -gangliosidosis patients, both of which are caused by β-GAL deficiency. Given the shared pathophysiological features of LSDs, the supraphysiological release of the therapeutic enzyme by gene-corrected hematopoietic cells may facilitate metabolic correction of both skeletal and brain cells, suggesting a potential expansion of the patient population that could benefit from the proposed treatment.

MATERIALS AND METHODS
Human samples
Healthy donor and MPSIVB patients' fibroblasts were obtained from the Telethon Network of Genetic Biobanks (IRCCS Istituto G. Gaslini, Genova). mPB CD34$^+$ cells were purified from purchased apheresis products (Hemacare) using the CliniMACS CD34 Reagent System (Miltenyi Biotec). Human PB samples were obtained from healthy donors and an MPSIVB patient (protocol TIGET09/TIGET05) in accordance with local committee approval and with the Declaration of Helsinki.

In vitro HSPC transduction
For human cell transduction, G-CSF mPB CD34$^+$ cells purchased from STEMCELL were placed in culture on retronectin-coated non-tissue culture-treated wells (Takara, T100A) in CellGro medium (Cell Genix, 20814-0500) supplemented with the following cytokines: 60 ng/mL human interleukin-3 (hIL-3), 100 ng/mL human thrombopoietin, 300 ng/mL human stem cell factor (hSCF), and 300 ng/mL human FLT3-L (all from Cell PeproTech). After 22 ± 2 h of pre-stimulation, cells were transduced at a specific MOI with a single hit of LV for 14 ± 1 h in the same cytokine-containing medium in the presence of 8 μM CsH (Merck, SML1575), as transduction enhancer. After transduction, cells were collected, washed in PBS and plated for CFU assay and myeloid liquid culture. For murine cell transduction, HSPCs were purified from the BM of *Glb1–/–* mice (065435-JAX) following the Cell Depletion Kit manufacturer's instructions (Miltenyi Biotec, 130-090-858). Murine HSPCs were plated (1 × 10^6/mL) for 2 h-pre-stimulation in StemSpan Serum-Free Expansion Medium (STEMCELL Technologies, 09600), supplemented with 5 ng/mL murine SCF (mSCF), 10 ng/mL human FLT3, 50 ng/mL murine thrombopoietin (mTPO) and 10 ng/mL hIL-3 (all from PreproTech). Cells were transduced overnight with the different LVs at an MOI of 100. Transduced cells were washed in PBS and plated for CFU assay and liquid culture expansion.

CFU assay
Human transduced and untransduced HSPCs were plated in a methylcellulose-based medium (Methocult H4434; STEMCELL Technologies) (1,000 cells/plate). After 14 days, colonies were counted and scored for morphology into erythroid (BFU-E), myeloid (GM-CFU), and erythroid/myeloid (GEMM-CFU) colonies by light

microscopy. Single colonies were collected for VCN analysis digital droplet PCR. Murine transduced and untransduced HSPCs were plated in a murine specific methylcellulose-based medium (Methocult M3434; STEMCELL Technologies) (500 cells/plate). 14 days later, colonies were counted and collected for digital droplet PCR VCN analysis. For BFU-E colony detection, plates were incubated in a solution containing DAB (3% acetic acid and 30% H_2O_2, which stains hemoglobin-containing cells to allow discrimination of BFU-E precursors from unstained CFU-GM). The number of BFU-E colonies was determined by DAB (3% acetic acid +30% H_2O_2) staining of hemoglobin-expressing cells.

Myeloid liquid culture

Human transduced and untransduced HSPCs were cultured in Iscove's modified Dulbecco's medium (IMDM) (Corning, 10-016-CMR) supplemented with 10% fetal bovine serum (FBS) (Euroclone, ECS0180L), 300 ng/mL hSCF, 60 ng/mL hIL-6 and 60 ng/mL hIL-3 (all from PreproTech). Cells were passaged twice a week at a density of 0.5×10^6/mL and counted using the Bio-Rad TC20TM automated cell counter for growth curve determination. After 14 days of expansion, cells were collected for VCN, protein and gene expression analysis. Murine transduced and UT cells were expanded for 10 days in RPMI 1640 medium (Corning, 10-043-CVR), supplemented with 10% FBS (Euroclone, ECS0180L), 5 ng/mL mSCF, 10 ng/mL hFLT3, 50 ng/mL mTPO and 10 ng/mL hIL-3 (all from PreproTech). During the 10-day expansion cells were counted three times using the Bio-Rad TC20TM automated cell counter for growth curve determination and collected for VCN and protein analysis.

OC differentiation

OCs were differentiated from the myeloid progeny of untransduced and transduced human mPB CD34$^+$ cells. Myeloid cells (5×10^5) were plated in 200 µL of alpha-Minimum Essential Medium (Gibco, 22571020), supplemented with 10% FBS and the following cytokines: 25 ng/mL human recombinant macrophage CFSs; 50 ng/mL human recombinant receptor activator of nuclear factor kappa-B ligand (all from PreproTech). Half of the medium was changed twice a week for 10 days. OC differentiation was evaluated by TRAP assay using the Tartrate Resistant Acid Phosphatase (TRAP) Kit (Sigma-Aldrich, 387A-1KT), following the manufacturer's instruction, and by RT-qPCR expression of MMP9 and TRAP5b genes.

Determination of β-GAL activity

For intracellular β-GAL activity, protein extract was obtained by resuspending cell pellets in 50–150 µL of H_2O and 25″ sonication using the Sonoreaktor UTR200 (Hielscher). Protein concentration was determined using BCA Protein Assay kit (Bio-Rad, 5000006) using BSA standards (Thermo Fisher, 23209). 0.1–5 µg of protein extract diluted in 10 µL of 0.2% BSA was incubated with 20 µL of (0.1 M) 4-methylumbelliferil-β-D-galactopyranoside (4MU-β-gal) (Sigma-Aldrich, M1633) for 1 h at 37°C. For β-GAL activity in the extracellular medium, 10 µL of CM from UT cells and 10 µL of 1:5 diluted CM from transduced cells were incubated with 4MU-β-gal for 1 h at 37°C. For medium conditioning, myeloid human and murine cells

were at a concentration of 2×10^6/mL for 24 h, OCs were plated at a concentration of 0.5×10^6/mL for 24 h and CD4$^+$ T cells were plated at a concentration of 1×10^6/mL for 24 h. At the end of the reaction, 200 µL of stopping buffer (carbonate 0.5 M [pH 10.7], Triton X-100) were added to each sample and enzymatic activity was measured as fluorescence emission (450/10) using the FLUOstar Omega reader (BMG LABTECH). The level of enzymatic activity was calculated using the fluorescence emission based on known amount of 4-methylumbelliferone standards (nmol) and protein amount (mg). β-GAL activity was measured upon treatment with M6P (5 mM) (Sigma-Aldrich, M6876) for 3 h according to the described protocol. To correlate protein content and enzymatic activity in the CM untransduced and transduced (LV-Glb1 WT, LV-Glb1 C2C12, and LV-GLB1) HEK293T cells, a calibration curve was built upon testing the enzymatic activity of serial dilutions of a 10 µL solution containing known concentration of recombinant human (rh) (Biotechne, 6464-GH) or murine (rm) (Origene, TP509735) β-GAL. A logarithmic trendline best fitted results of rm β-GAL activity, while linear correlation best fitted rh β-GAL up to 350 nmol/mg/h. The resulting curves were used to calculate β-GAL protein concentrations based on measured enzymatic activity (Figure S4A).

In vivo biodistribution study

In vivo studies were conducted according to protocols approved by the San Raffaele Scientific Institute and Institutional Animal Care and Use Committee, adhering to the Italian Ministry of Health guidelines for the use and the care of experimental animals (IACUC 1246). NOD.Cg-Kit^{W-41J} Tyr$^+$ Prkdc^{scid}Il2rg^{tm1Wjl}/ThomJ (NBSGW) mice were purchased from The Jackson Laboratory (JAX:026497) and maintained in specific pathogen-free conditions at San Raffaele Scientific Institute SPF Animal Facility. Transduced and untransduced human HSPCs (1.95×10^5 cells resuspended in 200 µL of PBS) were infused into 6- to 8-week-old NBSGW mice by tail vein injection. Human cell engraftment was monitored by flow cytometry analysis of the PB at 8 and 16 weeks after transplantation, and in the BM and spleen at the end of the experiment (16 weeks). BM cells were also analyzed for vector integration (VCN) and β-GAL activity. PB, BM, and spleen samples were collected from transplanted mice and analyzed using a multi-parametric flow cytometry assay. In brief, after RBC lysis with ACK (STEMCELL Technologies, 07850), BM cells were stained with fluorescent antibodies against human CD45 APC (BioLegend, 304037), CD19 PE-Cy7 (BioLegend, 302216), CD56 BV510 (BioLegend, 318340), CD90 PE-Cy5 (BioLegend, 328112), CD38 APC-Cy7 (Biolegend, 303534), CD3 PE (BD Biosciences, 345765), CD34 FITC (BD Biosciences, 345801), and CD33 VioBlue (Miltenyi Biotec, 130-099-485). PB cells underwent to the same preparation process and were stained with fluorescent antibodies against human CD45 APC, CD19 PE-Cy7, CD56 BV510, CD13 PerCP-Cy5.5 (BioLegend, 30714), CD3 PE, CD34 FITC, and CD33 VioBlue. All stained samples were acquired through BD FACSCanto II (BD Bioscience) cytofluorimeter after Rainbow beads (Spherotech, RCP-30-5A) calibration and raw data were collected through DIVA software (BD Biosciences). Data were subsequently analyzed

with FlowJo software v.10.9 (BD Biosciences) and the graphical output was automatically generated through Prism 10.0.0 (GraphPad software). For β-GAL activity, BM cells (2×10^6) were lysed, and 0.3 μg of protein extract diluted in 10 μL of 0.2% BSA was incubated with 20 μL of 4MU-β-gal for 1 h at 37°C. After the addition of 200 μL of stopping buffer, the enzymatic activity was measured as fluorescence emission (450/10) at the FLUOstar Omega reader. The level of enzymatic activity was calculated on the protein amount and normalized for the corresponding VCN.

Immunofluorescence analysis

MPSIVB fibroblasts were plated at a confluence of $1.5 \times 10^4/cm^2$ on coverglass. The day after, MPSIVB fibroblasts were exposed for 12 h to the CM from UT and transduced cells (HEK293T + LV-human GLB1; HEK293T + LV-murine GLB1). After two washing in PBS, MSPIVB fibroblasts were fixed with PFA 4% and permeabilized for 10 min in PBS + 10% FBS + 0.1% Triton X-100. Blocking was performed in PBS + 10% FBS for 40 min and 1 h incubation with goat serum. Cells were stained overnight at 4°C with the following antibody mix: mouse anti-human GLB1 (1:500, R&D, MAB6464), rat anti-human LAMP1 (1:1,000, Santa Cruz Biotech, sc-19992), and chicken anti-human vimentin (1:2,000, LSbio, LS-C76822-100). The day after, cells were washed five times in PBS and incubated with Alexa Fluor secondary antibodies (Invitrogen, goat anti-mouse 546, goat anti-rat 488, goat anti-chicken 647). After five washing in PBS, nuclei were stained with Hoechst (1:10,000, Invitrogen, H3570) and coverglass were properly mounted using Fluoromount-G Mounting Medium (Invitrogen) for image acquisition Mounting medium Images were acquired using the Leica TCS SP5 Laser Scanning Confocal and analyzed by Fuji.

Transferrin recycling assay

Healthy donor and patient-derived fibroblasts were seeded on 96-well plates at a concentration of 8,000 cells per well and incubated at 37°C. Twenty-four hours later, cells were incubated with 50 μg/mL Alexa Fluor (AF)-488 conjugated transferrin at 37°C for 45 min to allow receptor/ligand internalization and AF488-transferrin release into early/recycling endosomes (Loading). Cells were subsequently incubated in medium containing 50 μg/mL of unlabeled transferrin to stimulate transferrin receptor recycling and the subsequent release of AF488-tranferrin (Washout). At 15 and 45 min after washout, cells were treated for 45 s with acid was solution (150 mM NaCl, 10 mM acetic acid, [pH 3.5]) to remove the AF-transferrin non-specifically bound to plasma membrane and fixed with 4% PFA for 7 min. Nuclei were counterstained stained with Hoechst 33342. AF488-transferrin fluorescence intensity/cell was measured in, at least, 30 fields per well, imaged with the Opera Phenix (PerkinElmer) with a 40× objective. Image analysis was performed using Signals Image Artist (PerkinElmer), Mann-Whitney test followed by Bonferroni correction for multiple comparison using GraphPad Prism v.8 was performed on the parameter and the Loading was considered as 100% of fluorescence whereas the fluorescence intensity of the other time points was plotted as percentage of loading.

Analysis of receptor-mediated and fluid phase endocytosis with Alexa Fluor-labeled BSA and dextran

Healthy donor and patient-derived fibroblasts were seeded on 96-well plates at a concentration of 8,000 cells per well and incubated at 37°C. 24 h later, cells were starved for 2 h in serum-free IMDM medium and then incubated in the same medium containing 100 μg/mL AF488-BSA for 3 h at 37°C. Cells were then fixed with 4% PFA for 7 min, nuclei were counterstained with Hoechst 33342. For fluid phase endocytosis assay, healthy donor and patient-derived fibroblasts were seeded on 96-well plates at a concentration of 8,000 cells per well and incubated at 37°C. Twenty-four hours later, cells were incubated with 100 μg/mL of AF568-dextran for 20 min at 37°C in complete medium and then fixed with 4% PFA for 7 min. Nuclei were counterstained with Hoechst 33342.

AF488-BSA or AF568-dextran number of spots/cell was measured in, at least, 30 fields per well, imaged with the Opera Phenix (PerkinElmer) with a 40× objective. Image analysis was performed using Signals Image Artist (PerkinElmer), the number of BSA spots per cell was obtained by dividing the number of the spots above the selected threshold by the number of nuclei and Mann-Whitney test using GraphPad Prism v.8 was performed.

Trafficking of M6PR

Healthy donor and patient-derived fibroblasts were seeded on 96-well plates at a concentration of 8,000 cells per well and incubated at 37°C. Twenty-four hours later, cells were incubated with 4 μg/mL of anti-human CI-MPR mouse monoclonal antibody (Novusbio, cat. no. NB300-514) for 30 min in complete medium then fixed for 5 min with methanol at −20°C. Cells were then permeabilised/blocked for 1 h with blocking buffer (0.05% saponin, 0.5% BSA 50 mM NH_4Cl in PBS 1×). The cells were then incubated for 1 h with AF488-conjugated anti-mouse antibody (1:400 in blocking buffer) and nuclei were counterstained with Hoechst 33342. The perinuclear index of M6PR was analyzed by Signals Image Artist (PerkinElmer); cytoplasm was segmented into two fixed regions (perinuclear and peripheral), and the mean intensity was measured in both areas. The perinuclear index was obtained by the ratio of the two mean intensities (perinuclear/peripheral).

Immunofluorescence analysis of M6PR/EEA1 colocalization

Healthy donor and patient-derived fibroblasts were seeded on glass coverslips at a concentration of 3.5×10^4 per well and incubated at 37°C at least for 24 h. Cells were then fixed with 4% PFA for 7 min, permeabilized/blocked for 1 h with blocking buffer and then incubated for 1 h with anti-M6PR (mouse monoclonal) and anti-EEA1 (rabbit polyclonal) primary antibodies diluted in blocking buffer. Cells were then washed three times in PBS 1× and incubated for 45 min with AF488 conjugated anti mouse and AF568-conjugated anti rabbit antibodies (1:400 in blocking buffer). Nuclei were counterstained with DAPI and then cells were washed twice with PBS 1× once with water and mounted with Mowiol. Cells were imaged with Eclipse CI microscope (Nikon, Japan) 60× oil-immersed objective 1.4 NA. The coefficient of colocalization was measured with ImageJ

by analyzing the intensity of M6PR in EEA1-positive spots (identified by thresholding and segmenting the image). Statistics analysis was performed using Mann-Whitney test using GraphPad Prism v.8.

Murine and human recombinant β-GAL endocytosis assay

Patient-derived fibroblasts were seeded on glass coverslips at a concentration of 3.5×10^4 per well and incubated at 37°C at least for 24. Cells were then starved for 2 h in serum-free IMDM and then incubated in the same medium containing 2 µg/mL of either murine recombinant (mrβ-GAL) or human recombinant (hrβ-GAL) GLB1 for 15 and 120 min.

Then a two-step immunofluorescence was performed. Cells were first fixed with PFA 4% for 7 min, permeabilized/blocked for 30 min in blocking buffer and then incubated for 1 h with anti-LAMP1 (rabbit polyclonal) primary antibody (1:2,000 in blocking buffer). Cells were then washed three times in PBS 1× and incubated for 45 min with AF488 conjugated anti-rabbit antibody (1:400 in blocking buffer) and cells were then washed twice with PBS 1×. Cell were fixed again for 5 min with 2% PFA, washed twice with PBS 1× and permeabilized for 10 min with 0.1% Triton X-100 in PBS 1×, washed for 5 min in blocking buffer and incubated over night with anti-GLB1 mouse monoclonal antibody (MAB6464). Cells were then washed three times in PBS 1× and incubated for 45 min with AF568 conjugated anti-mouse antibody (1:400 in blocking buffer). Nuclei were counterstained with DAPI and then cells were washed twice with PBS 1× once with water and mounted with Mowiol. Cells were imaged with Eclipse CI microscope (Nikon, Japan) 60× oil-immersed objective 1.4 NA. β-GAL endocytosis was measured as total intracellular fluorescence by ImageJ. Mann-Whitney test adjusted for Bonferroni correction for multiple comparisons using GraphPad Prism v.8 was performed.

Statistical analysis

Except when specifically indicated in the figure legends, data were expressed as median ± range. Each dot indicates an *n*, representing a biologically independent sample/animal/experiment. In the entire manuscript, Mann-Whitney test was performed to compare two independent groups. Bonferroni correction was applied in the case of multiple comparison. Analyses were performed using GraphPad Prism v.8. Differences were considered statistically significant at *$p < 0.05$, **$p < 0.01$. ns indicates not significant comparison.

DATA AND CODE AVAILABILITY

Data available on request.

ACKNOWLEDGMENTS

AUTHOR CONTRIBUTIONS

DECLARATION OF INTERESTS

SUPPLEMENTAL INFORMATION

Supplemental information can be found online at https://doi.org/10.1016/j.omtm.2024.101313.

REFERENCES

1. Caciotti, A., Donati, M.A., Boneh, A., d'Azzo, A., Federico, A., Parini, R., Antuzzi, D., Bardelli, T., Nosi, D., Kimonis, V., et al. (2005). Role of beta-galactosidase and elastin binding protein in lysosomal and nonlysosomal complexes of patients with GM1-gangliosidosis. Hum. Mutat. *25*, 285–292.

2. Caciotti, A., Cellai, L., Tonin, R., Mei, D., Procopio, E., Di Rocco, M., Andaloro, A., Antuzzi, D., Rampazzo, A., Rigoldi, M., et al. (2021). Morquio B disease: From pathophysiology towards diagnosis. Mol. Genet. Metab. *132*, 180–188.

3. Funderburgh, J.L. (2002). Keratan sulfate biosynthesis. IUBMB Life *54*, 187–194.

4. Caterson, B., and Melrose, J. (2018). Keratan sulfate, a complex glycosaminoglycan with unique functional capability. Glycobiology *28*, 182–206.

5. Tomatsu, S., Okamura, K., Maeda, H., Taketani, T., Castrillon, S.V., Gutierrez, M.A., Nishioka, T., Fachel, A.A., Orii, K.O., Grubb, J.H., et al. (2005). Keratan sulphate levels in mucopolysaccharidoses and mucolipidoses. J. Inherit. Metab. Dis. *28*, 187–202.

6. Yuskiv, N., Higaki, K., and Stockler-Ipsiroglu, S. (2020). Morquio B Disease. Disease Characteristics and Treatment Options of a Distinct GLB1-Related Dysostosis Multiplex. Int. J. Mol. Sci. *21*, 9121.

7. Stockler-Ipsiroglu, S., Yazdanpanah, N., Yazdanpanah, M., Moisa Popurs, M., Yuskiv, N., Schmitz Ferreira Santos, M.L., Ae Kim, C., Fischinger Moura de Souza, C., Marques Lourenço, C., Steiner, C.E., et al. (2021). Morquio-like dysostosis multiplex presenting with neuronopathic features is a distinct GLB1-related phenotype. JIMD Rep. *60*, 23–31.

8. Paschke, E., Milos, I., Kreimer-Erlacher, H., Hoefler, G., Beck, M., Hoeltzenbein, M., Kleijer, W., Levade, T., Michelakakis, H., and Radeva, B. (2001). Mutation analyses in 17 patients with deficiency in acid beta-galactosidase: three novel point mutations and high correlation of mutation W273L with Morquio disease type B. Hum. Genet. *109*, 159–166.

9. Abumansour, I.S., Yuskiv, N., Paschke, E., and Stockler-Ipsiroglu, S. (2020). Morquio-B disease: Clinical and genetic characteristics of a distinct GLB1-related dysostosis multiplex. JIMD Rep. *51*, 30–44.

10. Arash-Kaps, L., Komlosi, K., Seegraber, M., Diederich, S., Paschke, E., Amraoui, Y., Beblo, S., Dieckmann, A., Smitka, M., and Hennermann, J.B. (2019). The Clinical and Molecular Spectrum of GM1 Gangliosidosis. J. Pediatr. *215*, 152–157.

11. Regier, D.S., Tifft, C.J., and Rothermel, C.E. (1993). GLB1-Related Disorders. In GeneReviews((R)), M.P. Adam, J. Feldman, G.M. Mirzaa, R.A. Pagon, S.E. Wallace, L.J.H. Bean, K.W. Gripp, and A. Amemiya, eds.

12. Celik, B., Tomatsu, S.C., Tomatsu, S., and Khan, S.A. (2021). Epidemiology of Mucopolysaccharidoses Update. Diagnostics *11*, 273.

13. Lambourne, M.D., and Potter, M.A. (2011). Murine beta-galactosidase stability is not dependent on temperature or protective protein/cathepsin A. Mol. Genet. Metab. *104*, 620–626.

14. Zhang, S., McCarter, J.D., Okamura-Oho, Y., Yaghi, F., Hinek, A., Withers, S.G., and Callahan, J.W. (1994). Kinetic mechanism and characterization of human beta-galactosidase precursor secreted by permanently transfected Chinese hamster ovary cells. Biochem. J. *304*, 281–288.

15. Samoylova, T.I., Martin, D.R., Morrison, N.E., Hwang, M., Cochran, A.M., Samoylov, A.M., Baker, H.J., and Cox, N.R. (2008). Generation and characterization of recombinant feline beta-galactosidase for preclinical enzyme replacement therapy studies in GM1 gangliosidosis. Metab. Brain Dis. *23*, 161–173.

16. Chen, H.H., Sawamoto, K., Mason, R.W., Kobayashi, H., Yamaguchi, S., Suzuki, Y., Orii, K., Orii, T., and Tomatsu, S. (2019). Enzyme replacement therapy for mucopolysaccharidoses; past, present, and future. J. Hum. Genet. *64*, 1153–1171.

17. Krivit, W. (2004). Allogeneic stem cell transplantation for the treatment of lysosomal and peroxisomal metabolic diseases. Springer Semin. Immunopathol. *26*, 119–132.

18. Wraith, J.E. (2006). Limitations of enzyme replacement therapy: current and future. J. Inherit. Metab. Dis. *29*, 442–447.

19. Biffi, A. (2017). Hematopoietic Gene Therapies for Metabolic and Neurologic Diseases. Hematol. Oncol. Clin. North Am. *31*, 869–881.

20. Platt, F.M., and Lachmann, R.H. (2009). Treating lysosomal storage disorders: current practice and future prospects. Biochim. Biophys. Acta *1793*, 737–745.

21. Rossini, L., Durante, C., Marzollo, A., and Biffi, A. (2022). New Indications for Hematopoietic Stem Cell Gene Therapy in Lysosomal Storage Disorders. Front. Oncol. *12*, 885639.

22. Biffi, A., De Palma, M., Quattrini, A., Del Carro, U., Amadio, S., Visigalli, I., Sessa, M., Fasano, S., Brambilla, R., Marchesini, S., et al. (2004). Correction of metachromatic leukodystrophy in the mouse model by transplantation of genetically modified hematopoietic stem cells. J. Clin. Invest. *113*, 1118–1129.

23. Biffi, A., Montini, E., Lorioli, L., Cesani, M., Fumagalli, F., Plati, T., Baldoli, C., Martino, S., Calabria, A., Canale, S., et al. (2013). Lentiviral hematopoietic stem cell gene therapy benefits metachromatic leukodystrophy. Science *341*, 1233158.

24. Visigalli, I., Delai, S., Politi, L.S., Di Domenico, C., Cerri, F., Mrak, E., D'Isa, R., Ungaro, D., Stok, M., Sanvito, F., et al. (2010). Gene therapy augments the efficacy of hematopoietic cell transplantation and fully corrects mucopolysaccharidosis type I phenotype in the mouse model. Blood *116*, 5130–5139.

25. Gentner, B., Tucci, F., Galimberti, S., Fumagalli, F., De Pellegrin, M., Silvani, P., Camesasca, C., Pontesilli, S., Darin, S., Ciotti, F., et al. (2021). Hematopoietic Stem- and Progenitor-Cell Gene Therapy for Hurler Syndrome. N. Engl. J. Med. *385*, 1929–1940.

26. Tucci, F., Consiglieri, G., Cossutta, M., and Bernardo, M.E. (2023). Current and Future Perspective in Hematopoietic Stem Progenitor Cell-gene Therapy for Inborn Errors of Metabolism. Hemasphere *7*, e953.

27. Pontesilli, S., Baldoli, C., Rosa, P.A.D., Cattoni, A., Bernardo, M.E., Meregalli, P., Gasperini, S., Motta, S., Fumagalli, F., Tucci, F., et al. (2022). Evidence of Treatment Benefits in Patients with Mucopolysaccharidosis Type I-Hurler in Long-term Follow-up Using a New Magnetic Resonance Imaging Scoring System. J. Pediatr. *240*, 297–301.e5.

28. Fumagalli, F., Calbi, V., Natali Sora, M.G., Sessa, M., Baldoli, C., Rancoita, P.M.V., Ciotti, F., Sarzana, M., Fraschini, M., Zambon, A.A., et al. (2022). Lentiviral haematopoietic stem-cell gene therapy for early-onset metachromatic leukodystrophy:

long-term results from a non-randomised, open-label, phase 1/2 trial and expanded access. Lancet *399*, 372–383.

29. Consiglieri, G., Tucci, F., De Pellegrin, M., Guerrini, B., Cattoni, A., Risca, G., Scarparo, S., Sarzana, M., Pontesilli, S., Mellone, R., et al. (2024). Early skeletal outcomes after hematopoietic stem and progenitor cell gene therapy for Hurler syndrome. Sci. Transl. Med. *16*, eadi8214.

30. Soldi, M., Sergi Sergi, L., Unali, G., Kerzel, T., Cuccovillo, I., Capasso, P., Annoni, A., Biffi, M., Rancoita, P.M.V., Cantore, A., et al. (2020). Laboratory-Scale Lentiviral Vector Production and Purification for Enhanced Ex Vivo and In Vivo Genetic Engineering. Mol. Ther. Methods Clin. Dev. *19*, 411–425.

31. Follenzi, A., and Naldini, L. (2002). Generation of HIV-1 derived lentiviral vectors. Methods Enzymol. *346*, 454–465.

32. Petrillo, C., Thorne, L.G., Unali, G., Schiroli, G., Giordano, A.M.S., Piras, F., Cuccovillo, I., Petit, S.J., Ahsan, F., Noursadeghi, M., et al. (2018). Cyclosporine H Overcomes Innate Immune Restrictions to Improve Lentiviral Transduction and Gene Editing In Human Hematopoietic Stem Cells. Cell Stem Cell *23*, 820–832.e9.

33. Kornfeld, S. (1987). Trafficking of lysosomal enzymes. FASEB J. *1*, 462–468.

34. Braulke, T., and Bonifacino, J.S. (2009). Sorting of lysosomal proteins. Biochim. Biophys. Acta *1793*, 605–614.

35. van der Spoel, A., Bonten, E., and d'Azzo, A. (2000). Processing of lysosomal beta-galactosidase. The C-terminal precursor fragment is an essential domain of the mature enzyme. J. Biol. Chem. *275*, 10035–10040.

36. De Leonibus, C., Cinque, L., and Settembre, C. (2019). Emerging lysosomal pathways for quality control at the endoplasmic reticulum. FEBS Lett. *593*, 2319–2329.

37. Oslowski, C.M., and Urano, F. (2011). Measuring ER stress and the unfolded protein response using mammalian tissue culture system. Methods Enzymol. *490*, 71–92.

38. Kadowaki, H., Nagai, A., Maruyama, T., Takami, Y., Satrimafitrah, P., Kato, H., Honda, A., Hatta, T., Natsume, T., Sato, T., et al. (2015). Pre-emptive Quality Control Protects the ER from Protein Overload via the Proximity of ERAD Components and SRP. Cell Rep. *13*, 944–956.

39. Rubio, C.A., Weisburd, B., Holderfield, M., Arias, C., Fang, E., DeRisi, J.L., and Fanidi, A. (2014). Transcriptome-wide characterization of the eIF4A signature highlights plasticity in translation regulation. Genome Biol. *15*, 476.

40. D'Azzo, A., Hoogeveen, A., Reuser, A.J., Robinson, D., and Galjaard, H. (1982). Molecular defect in combined beta-galactosidase and neuraminidase deficiency in man. Proc. Natl. Acad. Sci. USA *79*, 4535–4539.

41. Verheijen, F.W., Palmeri, S., Hoogeveen, A.T., and Galjaard, H. (1985). Human placental neuraminidase. Activation, stabilization and association with beta-galactosidase and its protective protein. Eur. J. Biochem. *149*, 315–321.

42. Hiraiwa, M., Saitoh, M., Arai, N., Shiraishi, T., Odani, S., Uda, Y., Ono, T., and O'Brien, J.S. (1997). Protective protein in the bovine lysosomal beta-galactosidase complex. Biochim. Biophys. Acta *1341*, 189–199.

43. Visigalli, I., Delai, S., Ferro, F., Cecere, F., Vezzoli, M., Sanvito, F., Chanut, F., Benedicenti, F., Spinozzi, G., Wynn, R., et al. (2016). Preclinical Testing of the Safety and Tolerability of Lentiviral Vector-Mediated Above-Normal Alpha-L-Iduronidase Expression in Murine and Human Hematopoietic Cells Using Toxicology and Biodistribution Good Laboratory Practice Studies. Hum. Gene Ther. *27*, 813–829.

44. Ballabio, A., and Bonifacino, J.S. (2020). Lysosomes as dynamic regulators of cell and organismal homeostasis. Nat. Rev. Mol. Cell Biol. *21*, 101–118.

45. Settembre, C., Fraldi, A., Rubinsztein, D.C., and Ballabio, A. (2008). Lysosomal storage diseases as disorders of autophagy. Autophagy *4*, 113–114.

46. Gorelik, A., Illes, K., Hasan, S.M.N., Nagar, B., and Mazhab-Jafari, M.T. (2021). Structure of the murine lysosomal multienzyme complex core. Sci. Adv. *7*, eabf4155.

47. Ohto, U., Usui, K., Ochi, T., Yuki, K., Satow, Y., and Shimizu, T. (2012). Crystal structure of human beta-galactosidase: structural basis of Gm1 gangliosidosis and morquio B diseases. J. Biol. Chem. *287*, 1801–1812.

48. Sena-Esteves, M., Camp, S.M., Alroy, J., Breakefield, X.O., and Kaye, E.M. (2000). Correction of acid beta-galactosidase deficiency in GM1 gangliosidosis human fibroblasts by retrovirus vector-mediated gene transfer: higher efficiency of release and cross-correction by the murine enzyme. Hum. Gene Ther. *11*, 715–727.

49. Weismann, C.M., Ferreira, J., Keeler, A.M., Su, Q., Qui, L., Shaffer, S.A., Xu, Z., Gao, G., and Sena-Esteves, M. (2015). Systemic AAV9 gene transfer in adult GM1 gangliosidosis mice reduces lysosomal storage in CNS and extends lifespan. Hum. Mol. Genet. *24*, 4353–4364.

50. Salmon, P., Kindler, V., Ducrey, O., Chapuis, B., Zubler, R.H., and Trono, D. (2000). High-level transgene expression in human hematopoietic progenitors and differentiated blood lineages after transduction with improved lentiviral vectors. Blood *96*, 3392–3398.

51. Bluebird Bio, I. Gene Therapy for Patients Less than 18 Years of Age with Early Cerebral Adrenoleukodystrophy (CALD) without Matched Sibling Donor. bluebird bio, Inc press release.

52. Aiuti, A., Biasco, L., Scaramuzza, S., Ferrua, F., Cicalese, M.P., Baricordi, C., Dionisio, F., Calabria, A., Giannelli, S., Castiello, M.C., et al. (2013). Lentiviral hematopoietic stem cell gene therapy in patients with Wiskott-Aldrich syndrome. Science *341*, 1233151.

53. Biffi, A., Bartolomae, C.C., Cesana, D., Cartier, N., Aubourg, P., Ranzani, M., Cesani, M., Benedicenti, F., Plati, T., Rubagotti, E., et al. (2011). Lentiviral vector common integration sites in preclinical models and a clinical trial reflect a benign integration bias and not oncogenic selection. Blood *117*, 5332–5339.

54. Squeri, G., Passerini, L., Ferro, F., Laudisa, C., Tomasoni, D., Deodato, F., Donati, M.A., Gasperini, S., Aiuti, A., Bernardo, M.E., et al. (2019). Targeting a Pre-existing Anti-transgene T Cell Response for Effective Gene Therapy of MPS-I in the Mouse Model of the Disease. Mol. Ther. *27*, 1215–1227.

55. Morrone, A., Bardelli, T., Donati, M.A., Giorgi, M., Di Rocco, M., Gatti, R., Parini, R., Ricci, R., Taddeucci, G., D'Azzo, A., and Zammarchi, E. (2000). beta-galactosidase gene mutations affecting the lysosomal enzyme and the elastin-binding protein in GM1-gangliosidosis patients with cardiac involvement. Hum. Mutat. *15*, 354–366.

56. Hinek, A., Zhang, S., Smith, A.C., and Callahan, J.W. (2000). Impaired elastic-fiber assembly by fibroblasts from patients with either Morquio B disease or infantile GM1-gangliosidosis is linked to deficiency in the 67-kD spliced variant of beta-galactosidase. Am. J. Hum. Genet. *67*, 23–36.

57. Privitera, S., Prody, C.A., Callahan, J.W., and Hinek, A. (1998). The 67-kDa enzymatically inactive alternatively spliced variant of beta-galactosidase is identical to the elastin/laminin-binding protein. J. Biol. Chem. *273*, 6319–6326.

58. Capotondo, A., Milazzo, R., Politi, L.S., Quattrini, A., Palini, A., Plati, T., Merella, S., Nonis, A., di Serio, C., Montini, E., et al. (2012). Brain conditioning is instrumental for successful microglia reconstitution following hematopoietic stem cell transplantation. Proc. Natl. Acad. Sci. USA *109*, 15018–15023.